



# Uncertainties of fluxes and $^{13}\text{C} / ^{12}\text{C}$ ratios of atmospheric reactive-gas emissions

Sergey Gromov<sup>1,2</sup>, Carl A. M. Brenninkmeijer<sup>1</sup>, and Patrick Jöckel<sup>3</sup>

<sup>1</sup>Max Planck Institute for Chemistry, Mainz, Germany

<sup>2</sup>Institute of Global Climate and Ecology (Roshydromet and RAS), Moscow, Russia

<sup>3</sup>Deutsches Zentrum für Luft- und Raumfahrt (DLR), Institut für Physik der Atmosphäre, Oberpfaffenhofen, Weßling, Germany

Correspondence to: Sergey Gromov (sergey.gromov@mpic.de)

Received: 20 December 2016 – Discussion started: 10 January 2017

Revised: 6 May 2017 – Accepted: 1 June 2017 – Published: 13 July 2017

**Abstract.** We provide a comprehensive review of the proxy data on the  $^{13}\text{C} / ^{12}\text{C}$  ratios and uncertainties of emissions of reactive carbonaceous compounds into the atmosphere, with a focus on CO sources. Based on an evaluated set-up of the EMAC model, we derive the isotope-resolved data set of its emission inventory for the 1997–2005 period. Additionally, we revisit the calculus required for the correct derivation of uncertainties associated with isotope ratios of emission fluxes. The resulting  $\delta^{13}\text{C}$  of overall surface CO emission in 2000 of  $-(25.2 \pm 0.7)\text{‰}$  is in line with previous bottom-up estimates and is less uncertain by a factor of 2. In contrast to this, we find that uncertainties of the respective inverse modelling estimates may be substantially larger due to the correlated nature of their derivation. We reckon the  $\delta^{13}\text{C}$  values of surface emissions of higher hydrocarbons to be within  $-24$  to  $-27\text{‰}$  (uncertainty typically below  $\pm 1\text{‰}$ ), with an exception of isoprene and methanol emissions being close to  $-30$  and  $-60\text{‰}$ , respectively. The isotope signature of ethane surface emission coincides with earlier estimates, but integrates very different source inputs.  $\delta^{13}\text{C}$  values are reported relative to V-PDB.

## 1 Introduction

Next to the kinetic chemistry implementation, magnitude and distribution of emissions of airborne compounds constitute perhaps the most crucial aspect of a modelling system dealing with the chemical state of Earth's atmosphere. A consistent emission set-up, in turn, requires (i) a careful selec-

tion of the emission inventories, (ii) adequate approaches to special cases (e.g. boundary conditions for the long-lived species) and, no less important, (iii) estimates of the pertinent uncertainties. The latter, typically being largest in comparison to the other sources of error in the model (such as for instance reaction rate coefficients), are often disregarded when the resulting simulated mixing ratios are reported. Often the inferred variation (temporal or spatial) of the species' abundance is quoted, which, however, does not represent an adequate uncertainty estimate. The situation becomes more complicated if the isotope-resolved emissions are to be used (i.e. fluxes separated using the information on the isotope ratios of the emitted compounds). For instance, which factors determine a particular emission source isotope ratio? How do these (and their respective uncertainties) influence the uncertainties of the underlying fluxes? And finally, what is the contribution of the emission uncertainties to the overall uncertainties of the simulated mixing/isotope ratios?

The above-mentioned issues and questions interested us in the course of the implementation of a fully  $^{13}\text{C} / ^{12}\text{C}$ -resolved comprehensive trace gas atmospheric chemistry study with the ECHAM/MESSy Atmospheric Chemistry (EMAC) model (Jöckel et al., 2006, 2010), particularly for the stable carbon isotope extension of its emission set-up, which we communicate in this paper. The reader is referred to the preceding phases of this model development, viz. the isotope extension of the kinetic chemistry submodel MECCA (Module Efficiently Calculating the Chemistry of the Atmosphere) and its application in simulating the carbon and oxygen isotope composition of gas-phase constituents

within the CAABA (Chemistry As A Boxmodel Application) atmospheric box model (Sander et al., 2011; Gromov et al., 2010). Both EMAC (which embodies an atmospheric chemistry general circulation model, AC-GCM) and CAABA serve as base models within the Modular Earth Submodel System (MESSy, Jöckel et al., 2005) that we employ. The overarching aim of our studies is a consistent simulation of the isotopic composition of atmospheric carbon monoxide (CO). A handful of modelling studies dedicated to CO isotopes exist to date (see the review by Brenninkmeijer et al., 1999) and have proven to yield deeper insights into their budget. However it leaves questions on missing atmospheric  $^{13}\text{C}$  in models (see Sect. 4). We therefore attempt to revisit this issue in a detailed and more comprehensive framework of the EMAC model, which we will communicate in subsequent papers. In addition to CO, the current study provides a bottom-up assessment of the emission  $^{13}\text{C}/^{12}\text{C}$  isotope ratios for the suite of other carbonaceous compounds, information that we believe will be useful for other isotope-enabled (modelling) studies focussing on them. For further information we refer to Brenninkmeijer et al. (2003), Goldstein and Shaw (2003) and Gensch et al. (2014), who review the benefits of using stable isotope ratios in atmospheric trace gases considered in this work.

The paper consists of three main parts. In the first part (Sect. 2), we briefly reiterate the implementation of the trace gas emissions in the evaluation set-up of the EMAC model (MESSy Development Cycle2, Jöckel et al., 2010, referred to hereafter as EVAL<sub>2</sub>) and supplement it with the formulation used to separate isotope emission fluxes. Furthermore, we derive some practical approaches with which to calculate combined flux/isotope ratio uncertainties of emissions in Sect. 2.2. The second part (Sect. 3) revisits proxies for signatures ( $^{13}\text{C}/^{12}\text{C}$  isotope ratios) of particular emission sources for CO, non-methane hydrocarbons (NMHCs), biogenic volatile organic (VOCs) and other carbonaceous compounds represented by EMAC. Special focus is on CO (the tracer of our primary interest) and its precursors. Finally, in the last part (Sect. 4) we summarise the results and discuss our estimates in comparison with previous studies. We recapitulate our results in Sect. 5 with concluding remarks.

## 2 Emission processes in EMAC

The emission of trace gases in EMAC is treated by the submodels OFFEMIS (formerly OFFLEM), ONEMIS (formerly ONLEM) and TNUDGE, which embody offline and online emission processes, and a pseudo-emission approach (tracer nudging), as detailed by Kerkweg et al. (2006). The offline emission process embodies a prescribed (precalculated) tracer flux into the atmospheric reservoir at the surface layer(s) or, for instance for the emission from air transportation sector, at the respective altitudes. This type of emission does not require a parameterisation dependent on the model

parameters. The EVAL<sub>2</sub> set-up includes the emissions from data sets comprising the following categories:

- anthropogenic emissions, based on the EDGAR emission inventory (detailed in Sect. 3.1),
- biomass burning emissions (GFED project database, second version; see Sect. 3.2), and
- biogenic emissions based on the OLSEN/GEIA databases (see Sect. 3.3).

Various key assumptions determine the emission isotopic signatures. Depending on the specific emission category, each of the data sets requires separate preprocessing for the isotopic extension. These are described in Sects. 3.1–3.5.

The online emissions, in contrast, are calculated during the runtime and require some of the model variables (e.g. surface temperature or precipitation) to calculate the resulting emission flux at the given model time step. For example, online emission suits for parameterisation of the trace gas emissions related to the biosphere–atmosphere interaction processes. In particular, the EVAL<sub>2</sub> set-up includes the online emissions of VOCs (isoprene/monoterpenes) from plants (see below, Sect. 3.3.1), which were scaled to achieve net yearly emissions of 305–340Tg(C) of isoprene (see Pozzer et al., 2007, Supplement). With this adjustment, more realistic mixing ratios of isoprene in the boundary layer are achieved in EMAC simulations.

At last, the pseudo-emission approach (tracer nudging) is a technique that performs the relaxation of the mixing ratios of sufficiently long-lived tracers towards prescribed (in space/time) fields. In the EVAL<sub>2</sub> set-up, these are the zonal averages of the observed mixing ratios of CH<sub>4</sub>, chlorinated hydrocarbons (CH<sub>3</sub>CCl<sub>3</sub>, CCl<sub>4</sub>, CH<sub>3</sub>Cl) and CO<sub>2</sub> which are used as the lower boundary conditions (surface layer) in the model. The isotopic separation of these pseudo-emission fields is described below in Sect. 3.5.

Further details of the emission processes implementation in EMAC and the corresponding model parameterisations are given by Kerkweg et al. (2006), Jöckel et al. (2006, 2010), Pozzer et al. (2007, 2009). In the next sections we describe chiefly the choice of the isotope emission signatures for the model set-ups including stable carbon isotopes.

### 2.1 Individual fluxes of isotopologues

The isotopic extension procedure consists of the separation of the total (i.e. sum of the abundant and rare isotope bearing) species fluxes into the individual isotopologues fluxes, accounting for the given isotopic ratio and thus the isotope content of a given species. Additionally, the consistency between the total flux and the sum of isotopically separated fluxes is verified. The rare isotopologues fluxes are calculated by weighting the total species flux with the respective

fractions  $^{\text{rare},i}f$  according to

$$^{\text{rare},i}f = \frac{{}^iR \cdot q}{1 + \sum_j {}^jR}, \quad {}^iR = (\delta^i + 1) \cdot {}^iR_{\text{st}}. \quad (1)$$

Here,  $q$  is the number of atoms of the selected isotope in a given species molecule, index  $j$  cycles all rare isotopologues (e.g.  $^{13}\text{CO}$  for stable C,  $\text{C}^{17}\text{O}$  and  $\text{C}^{18}\text{O}$  for stable O substitutions of CO),  ${}^iR$  is the isotopic ratio of a particular isotope  $i$  in the flux,  ${}^iR_{\text{st}}$  is the reference standard isotope ratio. When accounting for multiple rare isotopes, all ratios are required for the correct calculation of the resulting fraction of each of the isotopologues. The abundant isotopologue flux fraction, in turn, is calculated as

$$^{\text{abun}}f = 1 - \sum_j ^{\text{rare},j}f, \quad (2)$$

thus assuring that the sum of isotopically separated fluxes of the abundant and rare isotopologues equals the total flux value. The resulting fluxes  $F$  of the regular species and its isotopologues are

$$\begin{cases} ^{\text{abun}}F = F \cdot ^{\text{abun}}f \\ ^{\text{rare},i}F = F \cdot ^{\text{rare},i}f \end{cases} \\ F \equiv ^{\text{abun}}F + \sum_j ^{\text{rare},j}F. \quad (3)$$

For the sake of clarity, the molecular fractions  $f$  above are calculated plainly from the atomic content  $q$  and the isotopic ratios. The isotopic compositions of the emission fluxes, nevertheless, are conventionally (and within this study) reported using delta values  $\delta^i$ , which relate the isotope ratio  ${}^iR$  and the standard ratio  ${}^iR_{\text{st}}$  in Eq. (1). To express  $\delta^{13}\text{C}$  values (or “signatures”) the V-PDB scale with  ${}^{13}\text{C}R_{\text{st}}$  of  $11\,237.2 \times 10^{-6}$  (Craig, 1957) is used hereinafter (see Appendix A for details on choosing the  ${}^{13}\text{C}R_{\text{st}}$  value).

During the isotopic extension of the emission data, the preparation tools import the regular (total) emission fields (usually provided in netCDF format from <http://www.unidata.ucar.edu/software/netcdf/> with the flux values in units of molecules  $\text{m}^{-2}\text{s}^{-1}$ ), process these according to the given isotopic signatures and output fields containing the individual isotopologue fluxes. These in turn are read in by the model data import interface and utilised in a conventional way by the emission submodels (e.g. OFFEMIS). Depending on the source data used, the spatial resolution of the emission data sets varies. The input fields are transformed to the model grid during the model integration with the help of the NCREGRID submodel (Jöckel, 2006), which provides the consistent (flux-conserving) regridding algorithm.

## 2.2 Emission uncertainties analysis

It is desirable to estimate the uncertainties associated with the emission signatures for the subsequent analysis of the mod-

elling results, particularly in view of comparison with observational data. However, deriving the isotope composition uncertainties for composites of the various different sources with superimposed individual isotopic ratios is an intricate task. First, it should be clear how the uncertainties of the isotopic ratios are related, particularly in view of summing of several compartments (e.g. emission fluxes from different sources), all with their individual uncertainties for abundance and isotope composition. Second, the uncertainties associated with the amounts being summed are expected to influence the combined uncertainty of the ratio of the final aggregate, as a consequence of the law of error propagation. Even if the isotopic signature of each share (i.e. particular emission type) is determined (ideally) precisely, the non-zero uncertainties associated with the amounts of each share (i.e. emission fluxes) impose a non-zero uncertainty on the final isotopic signature of the total (emission). The approaches to calculating the combined emission and its isotope composition uncertainties are only sparingly documented in the literature; therefore they are derived below. The following analysis is based on the common practical fundament of uncertainties as described, for instance, by Drosig (2009) and Criss (1999).

Foremost, it is expedient to switch from using the relative isotopic composition to the actual equivalent ratio, i.e. from  $\delta^i$  to  ${}^iR$ . The use of delta variables would introduce impermeable complexities in subsequent calculations because in contrast to ratios, it is much more difficult to relate delta values to extensive quantities such as fluxes. The relation of the uncertainty  $\langle \delta^i \rangle$  reported for the delta value  $\delta^i$  to the uncertainty  $\langle {}^iR \rangle$  of the corresponding ratio  ${}^iR$  is

$$\langle {}^iR \rangle = \left( \frac{d\delta^i}{d{}^iR} \right) \Delta\delta^i = {}^iR_{\text{st}} \cdot \langle \delta^i \rangle. \quad (4)$$

Here and later on, the notation from Eqs. (1) to (3) is applied. For clarity the angle brackets  $\langle \rangle$  are introduced in place of the conventional  $\Delta$  to denote the uncertainty values. The  $\delta$ -value uncertainty is linearly proportional to the ratio uncertainty with the reference standard ratio being the proportionality factor. The total emission flux  $F_e$  of a given species is an integral of the particular emission source fluxes  $F_s$ . Employing the same notation, the values of  $F_e$  and its isotopic ratio  ${}^iR_e$  are

$$F_e = \sum_s F_s, \\ {}^iR_e = \varphi \sum_s {}^iR_s \cdot F_s, \quad \varphi \equiv \left( \sum_s F_s \right)^{-1}. \quad (5)$$

The summation in Eq. (5) is performed over the emission sources using index  $s$ .  $\varphi$  is introduced for the sake of notation simplification. It is noteworthy that plain source fluxes  $F_s$  cannot be used if the summation is done over several species with a varying isotope element count in the molecule. In that case, fluxes and their individual uncertainties  $\langle F_s \rangle$  must be

reduced to mole or mass fractions of the element of interest, e.g.  $\text{kg}(\text{C}) \text{yr}^{-1}$  (see Criss, 1999, Sect. 1.4 for details).

It is important for the applied method to differentiate whether or not the uncertainties associated with the magnitude of the individual emission fluxes and/or isotope ratios are correlated, that is, the various given estimates depend on each other. Examples of such are inverse modelling and other top-down approaches which may intrinsically correlate the fluxes from different emission sources by distributing their shares to the given (isotope mass-balanced) integral. Using any inverse modelling framework commonly requires the analysis of the posterior solution distribution, e.g. via an analytical solution, a systematic study of cases or a Monte Carlo study (see the review in Enting, 2002, Sect. 3.2). As pointed out by Tarantola (2005) (Sect. 3.3), at least a trivial estimate of the uncertainties' correlation is always possible. We note beforehand that no such estimates were provided in the inverse modelling studies regarded here (see below Sect. 4). Therefore, we are to gauge the upper limit (the “worst case”) of their uncertainties by assuming them to be correlated. The bottom-up estimates, on the contrary, are typically derived using independent proxies (e.g. country fuel usage statistics, satellite-derived mass of burned matter). Often uncertainties of assumptions (for example, if the emission comes predominantly from a particular plant material characterised by the distinct isotope signature) cannot be quantified using a strict mathematical apparatus; hence it should be analysed in a sensitivity framework. In other cases, the combined uncertainty accounting for the error propagation is calculated using the total differential of the function describing the product, in forms which are different for the correlated and uncorrelated estimates. Thus, the combined uncertainty  $\langle F_e \rangle$  of the total emission  $F_e$  in Eq. (5), expressed through the uncertainties of correlated (inferred top-down) components  $\langle F_s \rangle$  of individual sources  $F_s$ , is

$$\langle F_e \rangle = \sum_s \left| \frac{\partial F_e}{\partial F_s} \right| \cdot \langle F_s \rangle = \sum_s \langle F_s \rangle, \quad (6)$$

i.e. a simple (linear) addition of the individual uncertainties. In the case of uncorrelated (estimated bottom-up) total flux components, the resulting combined uncertainty is derived using the quadratic form of Eq. (6), which yields the square root of the sum of squared components  $\langle F_s \rangle$ :

$$\langle F_e \rangle = \sqrt{\sum_s \langle F_s \rangle^2}. \quad (7)$$

Analogously, the combined uncertainty  $\langle R_e \rangle$  for the resulting total emission isotope ratio  $R_e$  is calculated from both flux components ( $F_s \pm \langle F_s \rangle$ ) and ratio components ( $R_s \pm \langle R_s \rangle$ ) (index  $n$  varies similarly to  $s$ , enumerating the sources):

$$\begin{aligned} \langle {}^i R_e \rangle &= \sum_s \left( \left| \frac{\partial {}^i R_e}{\partial F_s} \right| \cdot \langle F_s \rangle + \left| \frac{\partial {}^i R_e}{\partial R_s} \right| \cdot \langle {}^i R_s \rangle \right) \\ &= \sum_s \left( |\varphi^2 \cdot \sum_n F_n ({}^i R_s - {}^i R_n)| \cdot \langle F_s \rangle + |\varphi \cdot F_s| \cdot \langle {}^i R_s \rangle \right) \end{aligned} \quad (8)$$

for the correlated case. The first term of the final sum in Eq. (8) describes the uncertainty in the isotope ratio arising purely from the uncertainty in emission strengths modified by the difference in the isotopic ratios between each pair of sources. The second term adds the uncertainties of the source isotope ratios weighted by the corresponding emission fluxes. In the case of uncorrelated estimates, the quadratic form of Eq. (8) yields the square root of a similar expression incorporating the above-mentioned terms squared:

$$\langle {}^i R_e \rangle = \sqrt{\sum_s \left( \frac{(\varphi^2 \cdot \sum_n F_n ({}^i R_s - {}^i R_n))^2 \cdot \langle F_s \rangle^2}{+(\varphi \cdot F_s)^2 \cdot \langle {}^i R_s \rangle^2} \right)}. \quad (9)$$

Equations (6)–(9) can be employed for the uncertainty estimation of any given combination of isotopic compartments, referring only to their abundances (or fluxes) and isotopic ratios. We remark here that using Eqs. (6)–(9) implies that the final combined uncertainties have a normal distribution about their mean values (i.e. standard deviations), although this may not be the case for individual emission flux estimates. Under the assumption of symmetricity for all individual uncertainties involved, however, normally distributed  $\langle {}^i R_e \rangle$  will be indeed the consequence of the law of uncertainty propagation (see D’Agostini, 2004 for details).

### 3 Proxies of emissions and their $^{13}\text{C} / ^{12}\text{C}$ ratios

#### 3.1 Anthropogenic emissions

The anthropogenic emissions in EVAL<sub>2</sub> are based on the EDGAR database (version 3.2 Fast Track 2000 (32FT2000), van Aardenne et al., 2005) as detailed by Pozzer et al. (2007). This inventory was compiled for the year 2000. It is noteworthy that, despite its complex structure (the emission is distributed to tens of various categories or “sectors”), the database has no seasonality; i.e. spatially distributed emission fluxes composing the emission are constant throughout the year. The inventory comprises approximately 40 sectors referring to the different anthropogenic emission sources (summarised in Table 1), which enables us to assign characteristic isotopic signatures individually to each sector. The influx is distributed to the surface and several near-surface model layers, depending on the emitted species and the emission sector. This serves to account for specific sources that deliver the pollutants to the various effective altitudes. The majority of sectors are associated with the surface and adjacent layers representing 45 and 140 m heights. The sources from power generation, industrial fuel usage and waste treatment sectors are represented with the various plume up-draughts distributed to the higher layers (spanning from 240 to 800 m above the ground). The detailed anthropogenic emission set-up and vertical distribution of the emission heights is described by Pozzer et al. (2009).

**Table 1.** Description of EDGAR FT32 emission source sectors and associated isotopic signatures.

Category	Source sectors	Emission activity	$\delta^{13}\text{C}$ [‰]
Biofuel combustion	B10, B20, B30, B40, B51	Industry, power generation, charcoal production, RCO*, road transport	$-25.0^g$ $-25.0^g$
Fuel combustion, production and transmission	F10, F20, F30, F40, F51, F54, F58, F60 <sup>d</sup> , F80, F90 <sup>c</sup> F57 <sup>a</sup>	Industry, power generation, conversion, RCO*, road/non-road transport, international shipping, international shipping, gas production Air traffic	$-27.5$ $-27.5^f$
Industrial	I10, I20 <sup>c</sup>	Iron and steel, non-ferrous metals	$-27.5^f$
	I30 <sup>c</sup> , I60 <sup>c</sup> , I70 <sup>c</sup> , I90 <sup>c</sup> , I50 <sup>b</sup>	Chemicals, food/beverages/tobacco, solvents, misc. industry, pulp and paper	$-27.5^f$
Land use <sup>b</sup>	L41, L42, L44, L47	(In)direct deforestation, savannah burning, vegetation fires	$-^a$
	L43	Agricultural waste burning	$-22.2^{e, g}$
Waste <sup>b</sup>	W40, W50 <sup>c</sup>	Waste incineration, misc. waste handling	$-24.0^{f, g}$

<sup>a</sup> Excluded from the set-up (or treated separately).

<sup>b</sup> Assuming a biomass burning-related emission source.

<sup>c</sup> Only CO emission (no VOCs).

<sup>d</sup> Only VOCs emission (no CO).

<sup>e</sup> For CO, a different signature of  $-21.3\%$  is used (see text).

<sup>f</sup> Fossil source assumed.

<sup>g</sup> Reflects the relative contribution of C<sub>3</sub> and C<sub>4</sub> plant material.

\* (Residential, Commercial and Other).

Table 1 lists the carbon isotopic signatures for CO and other emitted compounds assigned to the particular sector for anthropogenic emissions. Unfortunately, to date the information in the literature on the measured isotopic compositions of the different emitted compounds is scarce, particularly for NMHCs and other VOCs. Therefore, here the choice for the unknown signatures will follow the EDGAR categorisation, assuming the emission source material (e.g. crops, bio- or fossil fuels) and its characteristic processing (generally either biomass burning or high-temperature combustion) to determine the resulting isotopic ratio of the emitted tracer.

The least uncertain signature is for fossil fuel usage, most of which is on account of the transportation sectors. It is associated with an average characteristic composition of  $-27.5\%$  in  $\delta^{13}\text{C}$ , as reported for the world average engine exhaust CO by Stevens et al. (1972) and used as a proxy value here. Although quite diverse emitted CO isotope signatures were measured for various engine/fuel types (Kato et al., 1999a), any better assessment based on these signatures is not feasible, because the inventory does not provide the related information. The average value from Stevens et al. (1972) nonetheless agrees with more recent estimates. Thus, from measurements of CO isotopic composition in two cities in Switzerland, Saurer et al. (2009) infer the  $\delta^{13}\text{C}$  signature of the transportation source of  $-(27.2 \pm 1.5)\%$ , contrasting it with heavier CO emitted from local wood combustion sources. A similar transportation-emitted CO  $\delta^{13}\text{C}$  average value ensues from the observations in a Swiss highway tun-

nel study by Popa et al. (2014), viz.  $-(27.5 \pm 0.6)\%$  (the average  $\pm 2\sigma$  of the two Keeling plot-derived source  $\delta^{13}\text{C}$  signatures from the tunnel entrance and exit data is quoted).

Statistically insignificant variability in emission isotope ratios for transportation-related sources of selected NMHCs has been reported by Rudolph et al. (2002) with the signatures for the majority of species equating to within the measurement precision of  $2\%$  that of CO mentioned above. The exception of significant enrichment was found for ethyne (C<sub>2</sub>H<sub>2</sub>), which is not represented in the MECCA chemistry mechanism (as of EVAL<sub>2</sub> set-up) and may potentially constitute an enriched but very moderate source (see, for example, Ho et al., 2009). This is somewhat coherent with  $^{13}\text{C}$  enrichments found to accompany ethyne formation during the burning process (Czapiewski et al., 2002). We refer the reader to Gensch et al. (2014) for further details and a comprehensive review on a wide range of NMHC/VOC compounds. Altogether it is generally recognised that the fossil-related sources reflect the average isotopic ratios of the precursor crude oils. The aircraft emissions are associated with this source as well. However, the corresponding EDGAR emission (sector F57) is replaced by the inventory compiled by Schmitt and Brunner (1997) in EVAL<sub>2</sub>.

In analogy to the fuel combustion category (sector F), the same isotopic signature ( $-27.5\%$ ) is used for the industrial category (sector I). It is expedient to assume that those sources dominantly represent the fossil nature of the precursor carbon, as the emission is mainly associated with

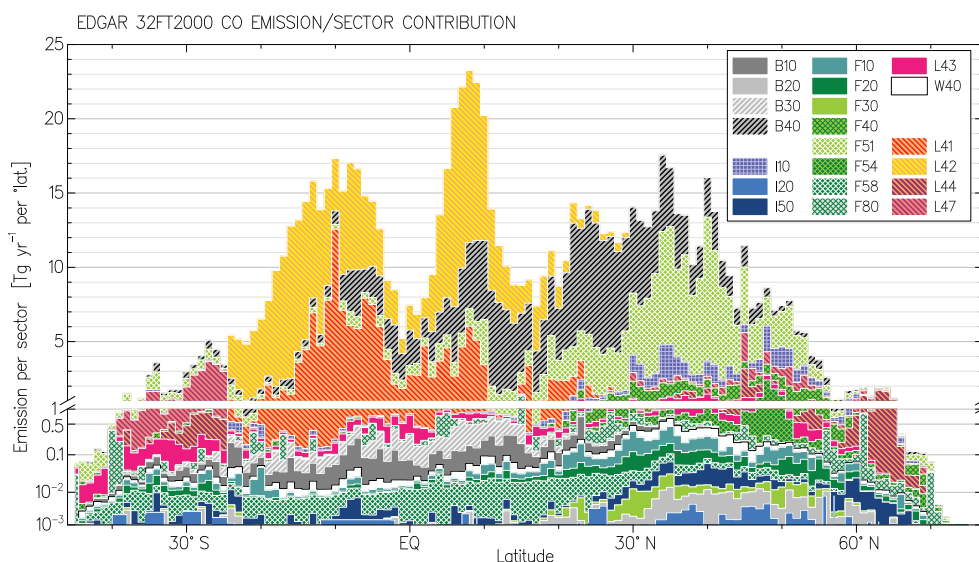


**Figure 1.** Relative contributions of emission sectors to the overall emission of CO in the EDGAR inventory. Values are given in  $\text{Tg}(\text{CO}) \text{yr}^{-1}$  per degree latitude. Note that the original EDGAR biomass burning sectors L41, L42, L44 and L47 are presented here for comparison only. They are being substituted (see text) by the GFED inventory. Note the change in ordinate axis scale at the value of unity.

the combustion of fuels in the majority of the industrial processes. An example is iron and steel production (sector I10), in which CO is emitted concomitantly during the thermal processing of the product in the furnaces (IISI, 2004). On the other hand, the influence of industrial sectors on the resulting emission signature should be minor, taking into account their small share in the overall anthropogenic emission. The comparison of the contributions of each EDGAR sector in the case of CO emission is presented in Fig. 1. Notably, the largest fluxes are associated with sectors B40 (biofuel consumption in the residential/commercial sector) and F51 (non- $\text{CO}_2$  combustion emissions from road transport); thus the input shares of these two sectors are decisive for the overall isotopic composition of CO in EDGAR. The total emission associated with industrial sectors amounts to  $34.5 \text{ Tg}(\text{CO}) \text{yr}^{-1}$ , which comprises approximately 6.3 % of the total anthropogenic source.

The less certain isotope signatures are associated, in turn, with the biofuel use (sector B) because of large uncertainties associated with the source influx estimates and somewhat unclear definition of this category itself. Although we presume that “biofuel use” in EDGAR predominantly refers to combustion of fuel wood and vegetable oils, the category includes industrial activities that may imply usage of fuels (e.g. liquid, gas, solid) produced from biomass (Olivier et al., 2002). To eliminate a potentially wrong association with the biofuel category, we discuss the isotope signatures of the woodfuel and waste/residue crops sources under the “biomass burning” category below. We remark that this activity likely comprises the major fraction of the biofuel use emissions related to heating and cooking in Asian and African regions (Yevich and Logan, 2003). No detailed information is available about

the biofuel production and use in other regions, however, particularly for the period for which the EDGAR inventory was compiled. Likewise, there are no specific measurements of the isotopic signatures of CO and other NMHCs/VOCs from biofuel sources reported yet (Goldstein and Shaw, 2003). These mainly comprise the use (primarily by combustion) of vegetable oil- and biomass-derived fuels, of which biodiesel and ethanol constitute the major parts (Demirbas, 2008). Although ethanol is included in the “biofuel combustion” category in EDGAR, neither the proportion of ethanol/biodiesel fuel sources nor the origin of precursor biogenic material are reflected in the inventory. A rough estimate of the isotopic signature is feasible nonetheless, assuming a certain average composition of the source biomass and negligible isotope effects accompanying the emission. On average, plant material is enriched in  $^{13}\text{C}$  with respect to fossil fuels and can be considered a composite of the carbon originating from two cardinal kinds of plant species, namely  $\text{C}_3$  and  $\text{C}_4$  plants (explained in detail in the following; see Sect. 3.3.1). Briefly, the isotopic compositions of those differ conspicuously owing to the differences in the photosynthesis mechanisms, yielding typical compositions of  $-27\text{‰}$  for  $\text{C}_3$  plants and  $-12\text{‰}$  for  $\text{C}_4$  plants (see, e.g. Dawson et al., 2002). The expected composition of the mixture is hence constrained by these values. Within the current study we follow Emmons et al. (2004) and adopt the value of  $-25\text{‰}$ , which corresponds to an approximate 4 : 1 ratio of  $\text{C}_3$ -to- $\text{C}_4$  plant material. There are, however, estimates that report a significantly higher fraction of  $\text{C}_4$  plants being used in global biofuel production. Thus, O’Connor (2009) quote the source plants species used for ethanol and biodiesel production. Whilst biodiesel is mainly produced from  $\text{C}_3$  species like soy, rapeseed, canola and

oil palm tree, ethanol is predominantly manufactured from corn and sugarcane, which are  $\text{C}_4$  crops. Projecting this partitioning on the gross production rates for the year 2000 (Demirbas, 2009) of  $156 \times 10^8$  and  $9.7 \times 10^8$  L for ethanol and biodiesel, respectively, will yield a rather high value for the average emission signature of  $-12.9\%$  for these fuels. Here, the fractionation associated with the fermentation process during the ethanol production is assumed to be negligible, although a few studies (Vallet et al., 1998; Zhang et al., 2003) indicate that the biogenic ethanol may be even slightly enriched with respect to the source material. A substitution of the reference biofuel  $\delta^{13}\text{C}$  signature of  $-25\%$  with the above-derived value of  $-12.9\%$  will result in an unlikely strong increase (greater than  $+8\%$ ) in the overall surface CO emission  $\delta^{13}\text{C}$  in eastern Asia and central Africa, compared to that for Europe and North America ( $+1.6$  and  $+1.1\%$ , respectively), where biofuel is being less extensively used. On a global scale, this enhancement reaches  $+4.6\%$ , zonally distributed as  $+6.1$  and  $+3.8/+2.1\%$  in the tropics and extratropical northern/southern hemispheres, respectively. The sensitivities to such substitution for the  $\delta^{13}\text{C}$  of NMHCs/VOCs emissions are lower, viz.  $+4.9\%$  (eastern Asia) and  $+2.8\%$  (central Africa) vs.  $+1.0$  and  $+0.8\%$  for Europe and North America, respectively, with a global average of  $+1.6\%$ . This rough analysis suggests that the sensitivity of simulated CO and NMHCs  $\delta^{13}\text{C}$  to biofuel  $^{13}\text{C}/^{12}\text{C}$  signature for Europe and North America will be likely below the (rather large) uncertainties associated with the biofuel category emission fluxes and isotope ratios themselves (see also Sect. 3.6 below).

The original biomass burning emission inventory of the EDGAR database (referring to land use, sector L) in the current set-up is substituted by the more comprehensive GFED inventory described in the following section, with the exception of the agricultural waste burning sector (L43), which is not included in GFED. The emission  $\delta^{13}\text{C}$  signature of  $-22.2\%$  is assigned to this source using the average composition of the burned material estimated for 2000 by Randerson et al. (2005). They use the  $\text{C}_3/\text{C}_4$  ratio of the burned vegetation inferred with the help of a vegetation-inclusive inversion-adjusted model and comparison with observed  $\text{CO}_2$  isotope ratios. A different signature of  $-21.3\%$  for CO is used, following the estimation similarly based on plant distribution, fuel loads and neglecting concomitant fractionations as described by Conny (1998). The estimates of burned plant composition by Randerson et al. (2005) do not consider the potential kinetic isotope effects that may escort biomass burning emission for various tracers.

Czapiewski et al. (2002) and later Komatsu et al. (2005) and Nara et al. (2006) report that  $\delta^{13}\text{C}$  of the major NMHCs emitted from biomass burning generally follows that of the fuel burnt, and the measurements did not reveal significant additional fractionations associated with the formation processes. Consequently, here (and further for the GFED data) the  $^{13}\text{C}$  isotope fractionation escorting burning process is

**Table 2.** Anthropogenic emission sources strengths and their isotopic signatures.

Species	Source [Tg(gas) yr <sup>-1</sup> ]			Totals	
	Biofuel	Fossils	Waste <sup>a</sup>	Emission <sup>b</sup>	$\delta^{13}\text{C}$ [‰]
CO	250.4	280.4	16.35	547.2/234.6	-26.2
CH <sub>3</sub> OH	6.58	3.13	0.43	10.14/3.80	-25.7
HCHO	3.50	0.98	0.23	4.71/1.88	-25.5
HCOOH	3.56	–	0.23	3.79/0.99	-24.9
C <sub>2</sub> H <sub>4</sub>	5.11	3.54	0.34	8.99/7.70	-26.0
C <sub>2</sub> H <sub>6</sub>	2.91	6.11	0.19	9.21/7.36	-26.6
C <sub>3</sub> H <sub>6</sub>	2.28	1.49	0.15	3.92/3.36	-26.1
C <sub>3</sub> H <sub>8</sub>	0.91	9.45	0.06	10.42/8.51	-27.2
C <sub>4</sub> H <sub>10</sub>	1.16	70.67	0.08	71.91/59.44	-27.4
CH <sub>3</sub> CHO	2.04	–	0.13	2.17/1.18	-24.9
CH <sub>3</sub> COOH	6.52	–	0.43	6.95/2.78	-24.9
CH <sub>3</sub> COCH <sub>3</sub>	1.89	3.18	0.12	5.19/3.16	-26.4
MEK	4.42	4.22	0.29	8.93/5.95	-26.1

<sup>a</sup> Refers to the EDGAR sector L43.

<sup>b</sup> Values are in [Tg(gas) yr<sup>-1</sup>]/[Tg(C) yr<sup>-1</sup>] units.

assumed to be negligible. On the contrary, the combustion conditions play a key role in the formation of CO during the biomass burning: normal ( $+0.5$  to  $+3.6\%$ ) and inverse ( $-2.1$  to  $-6.8\%$ )  $^{13}\text{C}$  fractionations were found to escort flaming and smouldering burning stages, respectively, with a further complex dependency on the burnt plant type (Kato et al., 1999b). The average composition of CO is rather expected to be depleted with respect to the source fuel, since CO emission is expected to be favoured in the smouldering phase (Yokelson et al., 1997). Unfortunately, the representation of the combustion stages in the emission data is limited; hence, one can provide only a qualitative estimate of the isotope effect (depletion). The quantitative estimates of the contributions from various stages (for instance, in the modelling study by Soja et al., 2004) could be improved with the use of the isotopic composition in this case. Conclusively, in contrast to the primary biomass burning sources, the emissions from the sector L43 induce a minor influence on the average CO emission signature, accounting for a total of  $16.3 \text{ Tg}(\text{CO}) \text{ yr}^{-1}$  (less than 3% of the total anthropogenic emission). In an analogous way, the waste treatment-related sources (sector W) are assigned to a slightly enriched composition of  $-24\%$  (compared to the average fossil fuel carbon) using the ratio of the biological to fossil carbon for waste incineration from Johnke (2000). It is assumed that the waste treatment category mainly refers to the waste incineration processes.

Table 2 lists the anthropogenic emissions and the compositions for the EDGAR database. The emissions for CO sum up to almost  $550 \text{ Tg yr}^{-1}$ , while the overall influx for the other trace gases amounts to approximately  $106 \text{ Tg}(\text{C}) \text{ yr}^{-1}$ . The mixing of the compositions of the main CO contributors, bio- and fossil fuel in the proportion of about 250 : 280,

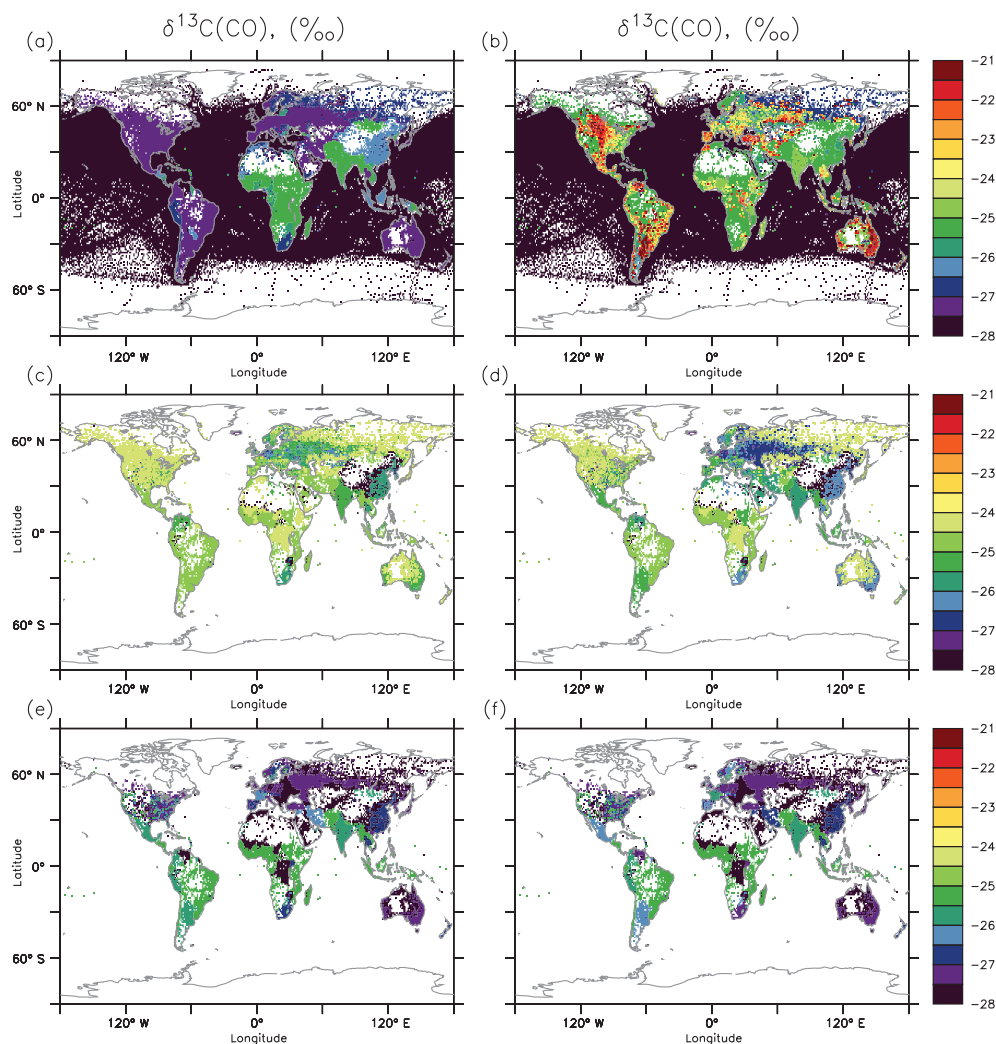


**Figure 2.** Stable carbon isotope composition of CO emitted from anthropogenic sources compiled on the basis of the EDGAR FT2000 inventory. Panels (a–f) refer to the specific emission heights of 45, 140, 240, 400, 600 and 800 m (see text for details).

yields the average composition of  $-26.15\%$ . This value is apparently sensitive to the assumed biofuel  $\delta^{13}\text{C}$  signature. The influence of the biofuel sources dominates for methanol, formaldehyde, formic acid, acetaldehyde and acetic acid, with values close to  $-25\%$ . Emitted alkanes and alkenes are enriched in  $^{13}\text{C}$  similar to CO, with an increasing influence of the fossil fuel input towards the higher hydrocarbons. The spatial distribution of the  $\delta^{13}\text{C}$  of anthropogenically emitted CO is depicted in Fig. 2, with the panels referring to the specific emission altitudes, as described above. The two lowermost layers subsume the majority of the emission sectors, including the shipping and biofuel-related sources (equally distributed to the layers) and fossil fuel sources (falling mainly in the surface layer). The emission signatures reflect the dominant biofuel emissions in Africa, eastern Asia and Oceania (Fig. 2a). In the second emission layer (Fig. 2b) the agricultural waste burning and waste incineration sources are re-

flected together with the biofuel emission. The overlying layers include the mixture of industrial and power generation sectors, with the latter prevailing in the top two layers.

### 3.2 Biomass burning emissions

The biomass burning emission data are prepared from the ORNL DAAC Global Fire Emission Database (GFED), version 2.1 inventory (Randerson et al., 2007, [http://daac.ornl.gov/VEGETATION/guides/global\\_fire\\_emissions\\_v2.1.html](http://daac.ornl.gov/VEGETATION/guides/global_fire_emissions_v2.1.html)), which is an updated and extended version of the initial GFED version 1 release (van der Werf et al., 2006) used in the EVAL<sub>2</sub> set-up (Pozzer et al., 2009). In the current set-up, monthly mean emission fields covering the period from 1997 to 2005 are used. The inventory includes emission fluxes for CO, NMHCs, nitrogen oxides ( $\text{NO}_x$ ) and other species; in addition, the estimation of the  $\text{C}_4$  plant carbon fraction of the burnt

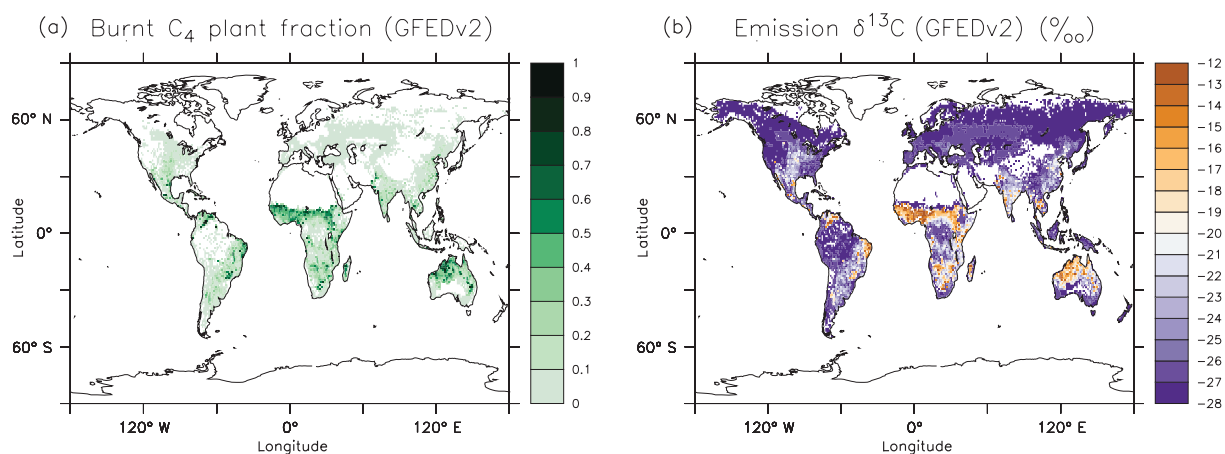


**Figure 3.** Burnt biomass  $\text{C}_4$  plant fraction (a) and corresponding isotopic signature of the emitted carbon (b) from the GFED v2.1 database. Fields are climatological yearly averages (see text, also Fig. 4).

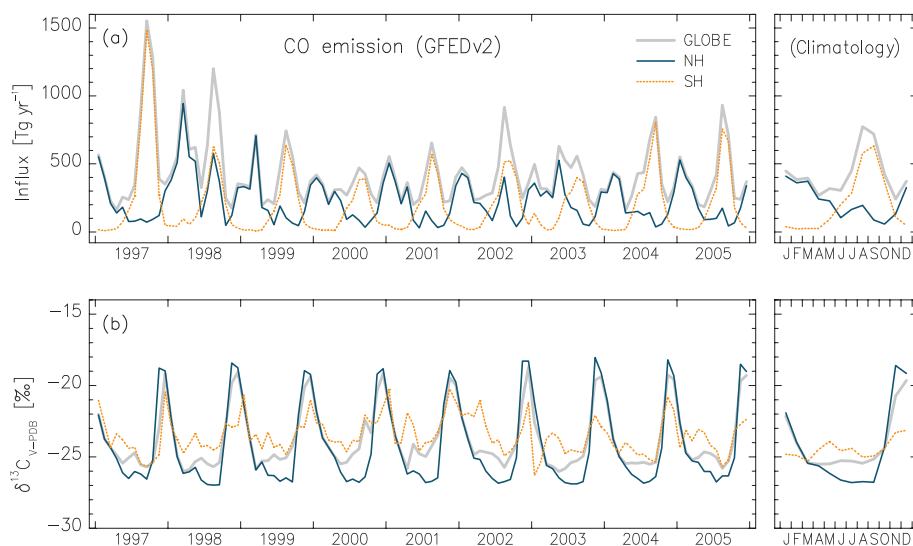


**Figure 4.** Emission of CO from biomass burning sources based on the GFED v2.1 data. (a) CO integrated flux in the Northern Hemisphere (NH), Southern Hemisphere (SH) and globally. (b) The carbon isotope composition of the respective fluxes. The right panels depict the climatological ensemble averages (shown in Fig. 3).

material is provided (Randerson et al., 2005). The latter is used to assign the isotopic signatures to the emission fluxes, assuming negligible isotopic fractionation during the burning, except for methanol ( $\text{CH}_3\text{OH}$ ), as discussed below. The resulting isotopologues fluxes are calculated as

$$\begin{cases} \frac{^{13}\text{C}F}{F} = (1 - f_{\text{C}_4}) \frac{q \cdot R_{\text{C}_3}}{R_{\text{C}_3} + 1} + f_{\text{C}_4} \frac{q \cdot R_{\text{C}_4}}{R_{\text{C}_4} + 1} \\ \frac{^{12}\text{C}F}{F} = (1 - f_{\text{C}_4}) \frac{(1 - q) \cdot R_{\text{C}_3} + 1}{R_{\text{C}_3} + 1} \\ + f_{\text{C}_4} \frac{(1 - q) \cdot R_{\text{C}_4} + 1}{R_{\text{C}_4} + 1}. \end{cases} \quad (10)$$

The notation follows that from Eq. (1) and  $f_{\text{C}_4}$  denotes the fraction of the burnt  $\text{C}_4$  plant material.  $F$  is the total emission

flux. Ratios  $R_{\text{C}_3}$  and  $R_{\text{C}_4}$  refer to the  $^{13}\text{C}$  isotope content associated with  $\text{C}_3$  and  $\text{C}_4$  plants, respectively; the corresponding isotopic signatures are discussed above. The emission is released into the near-surface model layer corresponding to 140 m height (see also Sect. 3.1).

For the sake of comparison presented here, an averaged (ensemble mean) yearly biomass burning climatology was derived, referring to the 2000–2005 period of the original data. The climatological yearly average spatial distribution of a burnt  $\text{C}_4$  biomass fraction and its translation into  $\delta^{13}\text{C}$  values of the emission are presented in Fig. 3. The heaviest (i.e. most enriched in  $^{13}\text{C}$ ) composition of the emission is associated with the grassland- and savannah-burning regions, where the  $\text{C}_4$  crops are most abundant.

**Table 3.** Biomass burning emission sources strengths and their isotopic signatures.

Species	Source [ $\text{Tg}(\text{gas})\text{yr}^{-1}$ ]			Average $\delta^{13}\text{C}$ [‰]	
	NH	SH	Total <sup>a</sup>	NH	SH
$\text{CO}^{\text{b}}$	223.2 (170.8–396.7)	202.8 (137.4–364.1)	425.9 (336.8–589.9)/ 182.6 (144.4–252.9)	–24.0 –(23.3–25.2)	–24.4 –(23.3–25.3)
$\text{CH}_3\text{OH}$	3.17	2.98	6.15/2.31	–36.7	–37.1
HCHO	1.69	1.58	3.27/1.31		
HCOOH	1.73	1.62	3.35/0.87		
$\text{C}_2\text{H}_4$	2.47	2.32	4.79/4.10		
$\text{C}_2\text{H}_6$	1.41	1.32	2.73/2.18		
$\text{C}_3\text{H}_6$	1.11	1.04	2.15/1.84		
$\text{C}_3\text{H}_8$	0.44	0.41	0.85/0.69	–24.3	–24.7
$\text{C}_4\text{H}_{10}$	0.56	0.52	1.08/0.89		
$\text{CH}_3\text{CHO}$	0.99	0.93	1.92/1.05		
$\text{CH}_3\text{COOH}$	3.16	2.97	6.13/2.45		
$\text{CH}_3\text{COCH}_3$	0.91	0.86	1.77/1.08		
MEK	2.14	2.00	4.14/2.76		

<sup>a</sup> Values are in [ $\text{Tg}(\text{gas})\text{yr}^{-1}$ ] and [ $\text{Tg}(\text{C})\text{yr}^{-1}$ ] units.

<sup>b</sup> For CO, interannual variation for 1997–2005 (yearly averages) is given in parentheses.

In Fig. 4 the temporal evolution of the hemisphere-integrated CO emission from biomass burning is presented. The markedly intensified emission rates in 1997–1998 are attributed to the increased forest and peat fires due to the droughts induced by the strong El Niño–Southern Oscillation climate pattern in those years (ENSO, Dube, 2009). Such an event is also notable (although less pronounced) for the years 2002–2003. Interestingly, ENSO activity is hardly reflected in the isotopic composition of the emission. However, the influence of the biomass source, which is especially important for its  $^{13}\text{C}$  enriched composition in the tropics and Southern Hemisphere (SH), increases without a doubt during El Niño years. The variation of the emission flux  $\delta^{13}\text{C}$  is twice as large in the Northern Hemisphere (NH) compared to that in the southern hemisphere. Such a difference arises from the large  $\text{C}_3$  plant extent at the northern high latitudes and the pronounced seasonal fire cycle. The summer/autumn extratropical fires in the NH occur predominantly in  $\text{C}_3$  plant communities, mainly in forests with an average composition of  $-27\text{‰}$ . In the wintertime the (sub)tropical sources take over, enriching the emission to the maximum of  $-19\text{‰}$  due to the large  $\text{C}_4$  plant fraction burnt in Africa and Asia. In the SH, the spatial diversity of the  $\text{C}_3 / \text{C}_4$  ratio is smaller over the smaller land extent, and the average signature varies around  $-24\text{‰}$  within  $\pm 1\text{‰}$  only.

The annual average biomass burning emission rates for the relevant species are listed in Table 3. In contrast to CO and  $\text{CH}_3\text{OH}$ , all NMHCs/VOCs emitted possess an equal isotopic composition because the fluxes for carbonaceous species are principally derived from the same burned carbon emission proxy (van der Werf et al., 2006). In order to obtain the individual tracer emission, the proxy is scaled with the

corresponding emission factor (conventions and values from Andreae and Merlet, 2001 are used), but the spatial distribution of the emission, hence  $\text{C}_3 / \text{C}_4$  carbon ratio, is the same. The difference in average hemispheric  $\delta^{13}\text{C}$  value amounts to  $0.4\text{‰}$  with the heavier emission in the SH. Compared to NMHCs/VOCs, the CO emission flux mapped onto the same burnt  $\text{C}_4$  plant fraction results in a slightly heavier ( $+0.3\text{‰}$  in  $\delta^{13}\text{C}$ ) average composition in GFED. An exceptional case amongst the NMHCs is  $\text{CH}_3\text{OH}$  which emitted significantly depleted  $^{13}\text{C}$  with respect to the material burned, as shown by Yamada et al. (2009). They attribute changes to the emission  $\delta^{13}\text{C}$  signature to the variations in the fraction of the precursor material (pectin vs. lignin methoxy pools; see also Keppler et al., 2004) and kinetic effects in loss processes. The overall depletion of  $\text{CH}_3\text{OH}$  with respect to the plant material is found to linearly correlate with the fire-modified combustion efficiency ( $\text{MCE} = \Delta\text{CO}_2 / (\Delta\text{CO} + \Delta\text{CO}_2)$ ,  $\Delta$  denotes trace gas concentration enhancement due to emission). Depletions of  $-(20\text{--}6)\text{‰}$  were measured within the studied range of MCE values of (85–98)%. Employing the relation provided by Yamada et al. (2009) and GFED-derived MCE we estimate the global average depletion of  $\text{CH}_3\text{OH}$  with respect to the plant material of  $-(12.4 \pm 0.8)\text{‰}$ , which corresponds to the average MCE value of  $(92.3 \pm 0.7)\%$ . The resulting methanol BB emission signature of  $-(36.9 \pm 2.2)\text{‰}$  in EMAC compares well with  $-(33 \pm 16)\text{‰}$  inferred by Yamada et al. (2009). Notably, the GFEDv2.1 inventory provides the combustion completeness parameter (CC) which is the estimate of the fraction of the actual fuel load combusted. Being similar to the MCE, CC might better reflect the burning stage conditions (i.e. flaming or smouldering phases). Unfortunately, the correspondence between these parameters

is not assessed to date; future applications of combustion completeness accounting for the kinetic isotope effects that escort biomass burning would be of great benefit.

### 3.3 Biogenic emissions

The biogenic emissions represent the discharge of organic species into the atmosphere associated with biosphere activity, particularly oceanic, soil and plant emissions. The current biogenic emission set-up in EVAL<sub>2</sub> follows Guenther et al. (1995) as described by Kerkweg et al. (2006), and comprises two parts for offline and online emissions (see the introduction in Sect. 2). The offline part was reassessed by Pozzer et al. (2007) and prescribes the emission for the large set of NMHCs/VOCs, excluding isoprene/monoterpenes emissions, which are calculated online. The data have a temporal resolution of 1 month, thus approximating the emission seasonal variation with no interannual variability. The emission is applied to the lowest model layer. The CO emission comprises in-place oxidation of some (non-industrial) hydrocarbons not accounted for in the applied MECCA chemistry (i.e. higher alkenes ( $C > 3$ ), terpene products other than acetone, higher aldehydes) and some direct CO emissions from vegetation and decaying plant matter. The oceanic CO emission strengths (monthly zonal distribution) are taken from Bates et al. (1995). No biogenic emissions for formaldehyde (HCHO), acetaldehyde ( $\text{CH}_3\text{CHO}$ ) and higher ketones (represented by methylethylketone (MEK) in MECCA) are included. The total annual emission strengths for CO and NMHCs/VOCs with the corresponding average compositions are listed in Table 4.

For the majority of the species, plant activity is the dominating biogenic emission. For a few species, viz. acetic acid ( $\text{CH}_3\text{COOH}$ ), formic acid (HCOOH) and ethene ( $\text{C}_2\text{H}_4$ ), the emission from the soils is estimated to be of comparable magnitude to the plant source (Kesselmeier and Staudt, 1999). Unfortunately, hardly any measurements or estimates of the isotopic composition of the soil-emitted carbon of these VOCs are available. The composition of precursor soil organic matter is also not well known (Boutton, 1991). Regarding the example of methane, which has microbial production in soils associated with large fractionations (Bréas et al., 2001), soil-emitted VOCs may constitute the source with the most uncertain signature. In the case of CO, the aggregate of soil emissions is estimated to be negligibly small compared both to soil sink and overall CO turnover (Sanderson, 2002); even a radical change in its signature will be hardly reflected in the average  $\delta^{13}\text{C}(\text{CO})$ .

A somewhat similar case arises with the oceanic emissions for which the strengths are debatable, and no isotopic signatures were estimated for NMHCs. Rudolph (1997) suggests the photochemical processing of dissolved organic carbon (DOC) to be the origin of C in the ocean-emitted NMHCs. Within the current set-up, an a priori signature of  $-20.5\%$

**Table 4.** Biogenic emission sources strengths and their isotopic signatures.

Species	Sources [Tg(gas) yr <sup>-1</sup> ]		Totals	
	Land (soils)	Ocean	Emission <sup>a</sup>	$\delta^{13}\text{C}$ [‰]
CO	100.0	12.7	112.7/48.3	-24.2
CH <sub>3</sub> OH	151.0 <sup>b</sup>	-	151.0/56.6	-64.8
HCOOH	5.58 (1.65)	-	5.58/1.46	-25.4 <sup>c</sup>
C <sub>2</sub> H <sub>4</sub>	10.0 (3.0)	0.91	12.13/5.19	-23.4
C <sub>2</sub> H <sub>6</sub>	-	0.54	0.54/0.22	-20.5
C <sub>3</sub> H <sub>6</sub>	2.15	1.27	3.41/2.92	-23.8
C <sub>3</sub> H <sub>8</sub>	-	0.35	0.35/0.29	-20.5
C <sub>4</sub> H <sub>10</sub>	-	0.40	0.40/0.33	-20.5
CH <sub>3</sub> COOH	3.39 (1.44)	-	3.39/1.36	-25.7
CH <sub>3</sub> COCH <sub>3</sub>	40.57	-	40.57/24.74	-25.7
DMS	0.91	-	0.91/0.35	-25.7
Isoprene <sup>d</sup>	346.0–385.4	-	346.0–385.4/ 305.1–339.7	-30.4 to -29.0

<sup>a</sup> Values are in [Tg(gas) yr<sup>-1</sup>] and [Tg(C) yr<sup>-1</sup>] units, respectively.

<sup>b</sup> Recommended updated value (Pozzer et al., 2007).

<sup>c</sup> Corrected for emission from formicine ants (0.22 Tg yr<sup>-1</sup>) of  $-19\%$  (Johnson and Dawson, 1993).

<sup>d</sup> Calculated online.

representing the marine isotopic carbon content (Avery Jr. et al., 2006, lower limit) is assigned. This value is somewhat higher than  $-22\%$  used for oceanic emissions by Stein and Rudolph (2007) in their modelling study on ethane isotopes. For CO, heavier oceanic emissions of  $-13.5\%$  are assumed, according to Manning et al. (1997). This value is based on the inverse modelling study and observations in the SH, where ocean input on CO is evidently significant. Quite contrary to this value, Nakagawa et al. (2004) estimate the ocean emitted CO to possess a rather depleted composition of  $-40\%$ . This value appears to be questionable; because the seawater-extracted CO was measured, the assumed precursor DOC composition was depleted (average of  $-31\%$ ) and the sampling was done in a single, fairly non-remote location in waters with high microbial activity (thus likely escorted with significant kinetic fractionation during the production). Finally, Bergamaschi et al. (2000) estimate the composition of CO emitted from the oceans to be as high as  $+5.1\%$  (scenario S2). Similar to biofuel-related sources, the oceanic CO is associated with a very uncertain isotopic composition. The change of this source signature from  $-13.5$  to  $-40\%$  will result in the decrease of the average biogenic emission signature by  $3\%$  with a corresponding  $0.3\%$  decrease in the overall CO surface emission composition.

#### 3.3.1 Plant emissions

For the biogenic emissions of plants, a novel approach referring to the physiological properties of plants is proposed here. In most previous (modelling) studies, the isotopic composition of the biogenically emitted tracers was based on the average global isotopic signature derived from the limited, often not consistent set of observations available. CO is a case in point here: the majority of the CO isotope modelling

studies assume a  $\delta^{13}\text{C}$  of CO emitted from the plant activity to be as low as  $-32.2\text{‰}$ , referring to the particular single estimate by Conny (1998). The latter was retrospectively derived from the observations at a rural US site (Stevens and Wagner, 1989), tolerating some important approximations, in particular (i) a two-component mixing model of the background and NMHC-only sources, (ii) constancy of the background composition throughout June to October, and (iii) neglect of the kinetic isotope fractionation caused by the CO sink. Whereas (i) is fairly applicable to the observations at a rural site, (ii) and (iii) rely on the 5-month constant background composition and neglect the variable input from the CO + OH reaction kinetic isotope effect (KIE). This is too rough an approximation, considering the intensive chemistry in the summer and characteristic CO lifetime that is shorter than a month. Indeed, the isotopic composition of background CO undergoes significant changes from spring to autumn, and the competition of the CO + OH reaction KIE and the varying in situ contribution from methane are the two non-negligible effects (Brenninkmeijer, 1993; Manning et al., 1997; Röckmann et al., 2002; Gromov et al., 2010).

Besides the temporal variation, the global average value does not represent the variable spatial distribution of the biogenic sources, which is important, since biogenic CO is mainly a product of the rapid oxidation of NMHCs. The latter, in turn, are expected to acquire specific isotopic ratios, being emitted from various plant species under different environmental conditions. The most studied compound in this respect is isoprene ( $\text{C}_5\text{H}_8$ ), one of the major biogenically released VOCs. Sharkey et al. (1991) measured the carbon isotopic composition of the emitted isoprene and found it to be dependent on the composition of the reservoir of recently fixed carbon ( $\text{CO}_2$  incorporated in the plant material during the initial step of the photosynthetic cycle). The isotope effects related to the plant activity and plant– $\text{CO}_2$  exchanges are extensively studied (see, for instance, Dawson et al., 2002). They usually operate with the isotope discrimination  $\Delta$ , a representative parameter describing the fractionation of the plant tissue relative to the atmospheric reservoir (Farquhar et al., 1989):

$$\Delta = \frac{\delta_a - \delta_p}{1 + \delta_p}, \quad (11)$$

where  $\delta_a$  and  $\delta_p$  refer to the isotopic composition of the air  $\text{CO}_2$  and plant tissues, respectively. In the form of Eq. (11), discrimination expresses the superposed effect of the various biological and physiological factors of plants, e.g. various plant metabolism pathways ( $\text{C}_3$  or  $\text{C}_4$ , indices 3 and 4 indicate the number of carbons in the initial fixation product molecule), water availability (response to droughts), solar irradiance or various stress factors. The contribution of each of them ought to be parameterised separately (Lloyd and Farquhar, 1994), which renders  $\Delta$  a complex parameter. The largest effect on  $\Delta$  is driven by the differences in the plant metabolism, the characteristic fixation mechanism

of air  $\text{CO}_2$  for subsequent photosynthesis. The majority of the terrestrial plants incorporate the  $\text{C}_3$  metabolism, when the fixation is escorted by the fractionation induced by RuBisCO (the specific enzyme used for the fixation in the photosynthetic Calvin cycle). Accounting additionally for the other fractionations (e.g. diffusion of  $\text{CO}_2$  through the stomata, etc.), typical  $\Delta$  values for  $\text{C}_3$  plants span from 15 to 25 ‰. Note that discrimination is expressed on the positive scale. Assuming a certain  $\delta_a$  (approximately  $-8\text{‰}$  for current air  $\text{CO}_2$ ) and using Eq. (11), one derives the  $\text{C}_3$  plant composition within the range of  $-32$  to  $-23\text{‰}$ .  $\text{C}_4$  plants employ other enzymes than RuBisCO; their efficiency is associated with lower  $\Delta$  values of 2.5 ‰ to 5 ‰, corresponding to a  $-10$  to  $-13\text{‰}$  range of plant material  $\delta^{13}\text{C}$ . In addition to  $\text{C}_3$  and  $\text{C}_4$  plants, a minor fraction of terrestrial CAM (crassulacean acid metabolism) plants exists. CAM can be regarded as a temporal coupling of  $\text{C}_3$  and  $\text{C}_4$  metabolisms employed by the plant for optimised adaptation to arid conditions. Therefore, CAM plants are characterised with a wide range of discriminations from 2 to 22 ‰ (Griffiths, 1992), or  $-10$  to  $-30\text{‰}$  expressed in  $\delta^{13}\text{C}$  of the plant tissue carbon. The specified plant biomass compositions result from the permanent isotopic equilibration with the atmospheric pool (i.e.  $\text{CO}_2$ ) accompanied by discrimination; thus the use of Eq. (11) is rational when the long-term value of  $\Delta$  is considered.

In view of the correlation between the emitted species isotopic composition and the plant isotope discrimination, the latter is assumed here as a proxy for biogenic emission signatures in the current emission set-up, rather than the global average signature. This approach, however, premises the following key assumptions:

- Few studies indicate that a moderate part (9–28 %, Schnitzler et al., 2004; Karl et al., 2002) of the emitted isoprene may be issued from a separate carbon source of the plant. Its composition may differ from that expected from  $\Delta$ , the photosynthetically fixed carbon. Moreover, neither the isotopic composition of the suggested alternative sources was deduced nor were the fractionations associated with their incorporation in the emission product. Affek and Yakir (2003) overcame this issue showing that the long-term value of  $\Delta$  may be used as a proxy for the average bulk leaf biomass value, thus concluding the depletion of the emitted isoprene with respect to the latter. It is important to note that the contribution of alternative sources becomes larger as the plant is put under stress (e.g. experiments of Schnitzler et al., 2004 were partly carried in  $\text{CO}_2$ -free air). For natural conditions, the proportion of the non-photosynthetically fixed carbon is likely to be smaller.
- The above-mentioned studies have exclusively analysed isoprene and methanol; no comparable measurements were performed regarding the other species. Nevertheless, there are isotopic compositions of biogenically

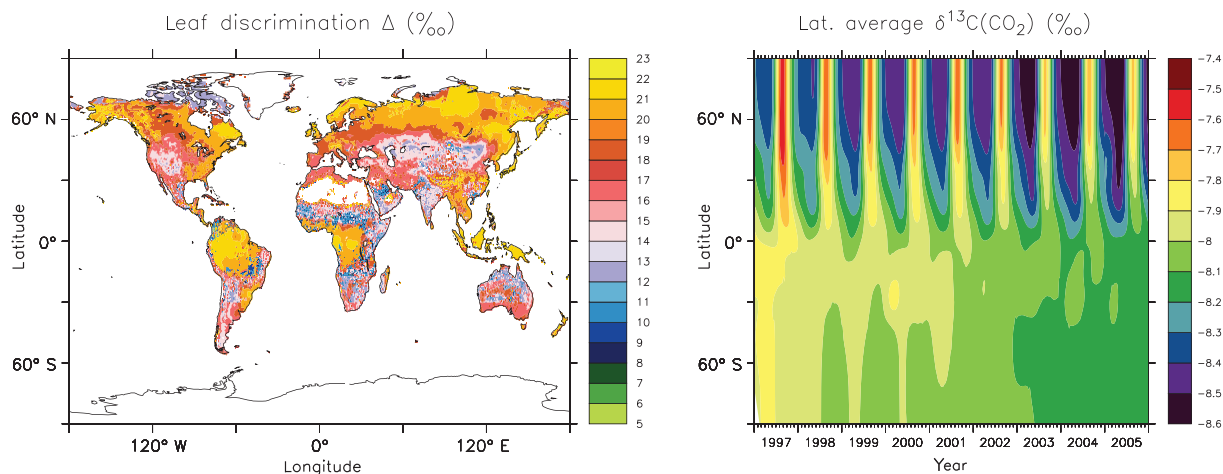


**Figure 5.** (a) Global mean leaf discrimination distribution (ISOLUCP experiment, Scholze et al., 2008). The distribution generally reflects the proportion of the  $\text{C}_3 / \text{C}_4$  metabolism and characteristic carbon photorespiratory fractionation in the various ecosystems, land use regimes and climate zones. (b) Time series of the latitudinal average surface isotopic composition of  $\text{CO}_2$  from the GLOBALVIEW-CO2C13 (2009) data.

emitted NMHCs/VOCs reported relative to the plant bulk leaf composition (Rudolph et al., 2003; Sharkey et al., 1991; Conny and Currie, 1996), as well as few measurements of the plant-emitted VOCs with comparable  $\delta^{13}\text{C}$  to that of the expected bulk composition (Giebel et al., 2010). Thus, it is practicable to derive the emission signatures from the measured depletions of the trace gas composition relative to that of the plant leaf. Under the assumption that the latter is determined by the long-term value of  $\Delta$  yielded from the specific plant metabolism and diffusion/equilibrium effects of the  $\text{CO}_2$  photosynthetic fixation and respiration, such an approach is tolerable.

To construct the emission signatures, the estimated global distribution of the leaf discrimination is taken from Scholze et al. (2008). They use a dynamic global vegetation model extended with the terrestrial isotopic carbon module. The parameterisation of the leaf carbon discrimination is based on the framework developed by Lloyd and Farquhar (1994) neglecting poorly understood fractionations in several processes involved in the photorespiration. The vegetation dynamics model accounts for the plant and soil carbon reservoirs and a set of numerous parameters including the vegetation composition, its productivity, fire disturbance, water availability and land use schemes, as well as climate forcing (monthly temperature, precipitation and cloud cover fields). For the detailed model description, the reader is referred to Scholze et al. (2003) and the above-mentioned references. The simulated leaf discrimination for the year 1995 from the ISOLUCP experiment (depicted in Fig. 5a) is adopted here. The characteristic variability of the global leaf discrimination magnitude is of the order of decades; thus the data referring to 1995 is reckoned to be consistent with the stud-

ied year 2000. The bulk leaf composition  $\delta_p$  is calculated straight from the isotope discrimination defined in Eq. (11), for which the isotopic composition of  $\text{CO}_2$ , namely  $\delta_a$ , is required. For the period of 1997–2005 (corresponding biomass burning data in the current set-up), the estimate of the surface  $\text{CO}_2$  isotopic composition from the GLOBALVIEW project (GLOBALVIEW-CO2C13, 2009) is taken. These data comprise latitudinal weekly averages (shown in Fig. 5b), and hence the latitudinal mean of the  $\delta^{13}\text{C}(\text{CO}_2)$  went into the calculations. Except for isoprene and methanol, the fractionations accompanying the emissions are considered to be negligibly small, as no significant deviation (within measurement standard deviation of 1‰) from the source plant material for the selected NMHCs was reported (Conny and Currie, 1996; Guo et al., 2009). For the fractionation escorting isoprene emission, the lower limit of 4‰ depletion relative to the bulk leaf composition from Affek and Yakir (2003) is taken. In the case of methanol, significantly larger depletions (about 40‰) were discovered by Keppler et al. (2004) and linked to highly depleted pectin and lignin methoxyl pools which plants likely use to produce  $\text{CH}_3\text{OH}$ . A later work by Yamada et al. (2010) confirmed similar fractionations for a different set of  $\text{C}_3$  plants species. Using data from both studies, we reckon the depletion of  $(39 \pm 6.3)\%$  with respect to the bulk composition of the plant for the emission of methanol from plants. Note that this value represents only two  $\text{C}_4$  and one CAM plant species out of total 18 species regarded in these studies.

The biogenic emission strengths and resulting isotopic signatures (average values for the year 2000) are listed in Table 4. The largest offline emissions pertain to CO and methanol. The final signatures reflect the proportion of the land (average  $-25.7\%$ ) and oceanic sources, with an ex-

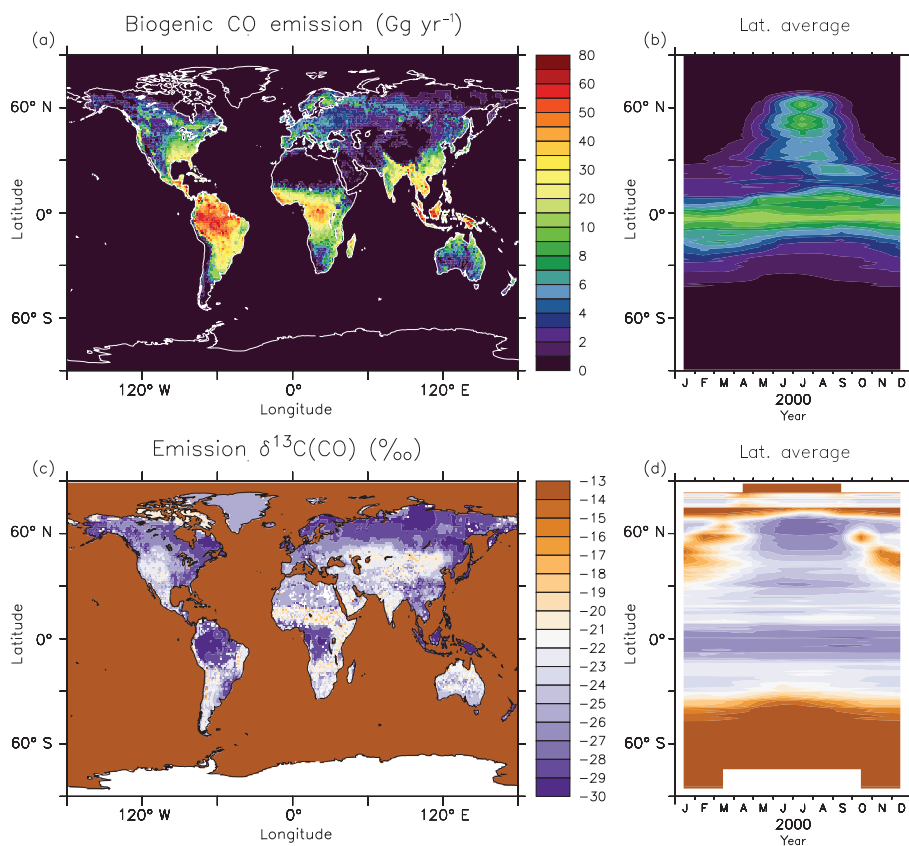


**Figure 6.** (a, c) CO emission from the biogenic sources (a) and corresponding isotopic signature (c). (b, d) Corresponding time series of latitudinal averages for the year 2000 emission with identical colour scales.

ception of much depleted methanol emission of  $-64.8\text{‰}$  in  $\delta^{13}\text{C}$ . The average composition of the CO emission of  $-24.2\text{‰}$  implies considerably lower  $^{13}\text{C}$  depletion compared to the previously assumed  $-32.2\text{‰}$  (Conny, 1998), which results in an effective increase of about  $+0.8\text{‰}$  in the overall surface emission  $\delta^{13}\text{C}$  value. The major part of the emissions is placed in the tropics, with the summer-triggered large emission in the NH. An example for CO is sketched in Fig. 6. The largest influx is associated with the areas of rather depleted sources. The land sources are comparable to the oceanic sources in NH winter, which is reflected in the zonal average  $\delta^{13}\text{C}$  of CO emission. Based on the same proxy, the dynamics of the emission  $\delta^{13}\text{C}$  value is similar for the other species.

The isoprene emission, in turn, is calculated on-line, utilising model parameters obtained during the calculation. The emission parameterisation is described by Ganzeveld et al. (2002) and implemented for EMAC in the ONEMIS (formerly ONLEM) submodel (Kerkweg et al., 2006). The key variables for the  $\text{C}_5\text{H}_8$  emission are the temperature and radiative balance over the canopy (both are provided by the base model) and the vegetation foliar density (prescribed). The isoprene influx is calculated at every model time step from the above-mentioned variables. To account for the iso-

topic  $\text{C}_5\text{H}_8$  emission, the necessary extension to ONEMIS was implemented. The influxes of the  $^{12}\text{C}$  and  $^{13}\text{C}$  isotopologues are calculated from the original isoprene emission flux and either simulated or prescribed average  $\text{CO}_2$  isotopic composition. The leaf discrimination distribution is imported as a parameter (similar to the other prescribed data fields). The overall  $\text{C}_5\text{H}_8$  emission ranges within  $350\text{--}380\text{ Tg yr}^{-1}$  with the corresponding average  $^{13}\text{C}$  signature within the range of  $-30.4$  to  $-29.0\text{‰}$  depending on seasonal and spatial emission flux variation. As indirect (in situ oxidation) source of CO, isoprene dominates over the sum of all remaining VOCs accounted for in the set-up.

### 3.4 Final composition of the surface sources

Table 5 lists the annually integrated trace gas emissions from the surface in the reference emission set-up of this study. For the carbonaceous species, stable carbon isotopic compositions resulting from the superposition of the various emission types are given; values refer to the year 2000. The inter-annual variation for 1997–2005 of the average  $\delta^{13}\text{C}$  signature of emitted CO is less than  $0.5\text{‰ yr}^{-1}$  resulting from the variability of  $\pm 0.6\text{‰ yr}^{-1}$  in the biomass-burned carbon and a negative trend in the  $\text{CO}_2$  composition in the last decades

**Table 5.** Surface emission sources in the EMAC (EVAL<sub>2</sub> set-up).

Species	Source [Tg(gas) yr <sup>-1</sup> ]			Aggregate uncertainty factor <sup>a</sup>	Totals (uncertainty)	
	Anthropogenic (includes biofuel)	Biomass burning	Biogenic		Emission [Tg(C) yr <sup>-1</sup> ] <sup>b</sup>	$\delta^{13}\text{C}$ [‰]
CO	547.2 (250.4)	425.9	112.7	1.17	465.6 ± 79.1	-25.2 ± 0.7
CH <sub>3</sub> OH	10.1 (6.6)	6.15	151.0	2.81	62.7 ± 113.2	-61.4 ± 3.6
HCHO	4.71 (3.50)	3.27	–	1.45	3.2 ± 1.5	-25.1 ± 1.1
HCOOH	3.79 (3.56)	3.35	5.58	1.92	3.3 ± 3.1	-25.0 ± 0.8
C <sub>2</sub> H <sub>4</sub>	8.99 (5.11)	4.79	10.9	1.84	21.1 ± 17.9	-24.4 ± 0.7
C <sub>2</sub> H <sub>6</sub>	9.21 (2.91)	2.73	0.54	1.44	10.0 ± 4.4	-25.9 ± 0.8
C <sub>3</sub> H <sub>6</sub>	3.92 (2.28)	2.15	3.42	1.54	8.1 ± 4.4	-24.4 ± 0.7
C <sub>3</sub> H <sub>8</sub>	10.4 (0.9)	0.85	0.35	1.62	9.5 ± 5.8	-26.8 ± 0.9
C <sub>4</sub> H <sub>10</sub>	71.9 (1.2)	1.08	0.40	1.72	60.7 ± 43.8	-27.3 ± 1.0
CH <sub>3</sub> CHO	2.17 (2.04)	1.92	–	1.51	2.2 ± 1.1	-24.7 ± 1.2
CH <sub>3</sub> COOH	6.95 (6.52)	6.13	3.39	1.58	6.6 ± 3.8	-24.9 ± 1.0
CH <sub>3</sub> COCH <sub>3</sub>	5.19 (1.89)	1.77	40.6	2.71	29.0 ± 49.6	-25.7 ± 0.8
MEK	8.93 (4.42)	4.14	–	1.42	0.7 ± 3.7	-25.6 ± 0.9
DMS	–	–	1.82	3.0	0.4 ± 0.7	-25.7 ± 1.0
C <sub>5</sub> H <sub>8</sub>	–	–	365.7	3.0	322.4 ± 644.8	-29.7 ± 1.0

<sup>a</sup> Derived from the final (composite) flux uncertainty using Eq. (12) (see Sect. 3.6).

<sup>b</sup> Mind the different units used for individual categories and total values, i.e. [Tg(gas) yr<sup>-1</sup>] and [Tg(C) yr<sup>-1</sup>], respectively.

(-0.02‰ to -0.03‰ yr<sup>-1</sup> due to the input of fossil fuel-derived carbon into the atmosphere, Yakir, 2011) propagating into the biogenic emissions.

The spatial distribution and annual dynamics of the surface CO emission is presented in Fig. 7. The largest emission is situated in the tropics, particularly in Africa and Asia, and attributed to the biomass burning season in July–September in the SH, African fires in December and high-latitude fires in Eurasia and Northern America from May to September. A substantial proportion made up by the anthropogenic sources has no distinct seasonality and is prominent in the NH high latitudes; these are mostly transportation and industry (i.e. fossil fuel related) sources. The relative dynamics of the isotopic composition is weaker than that of the corresponding flux magnitudes, indicating that the dominant sources are close to the average -25 to -27‰ of terrestrial carbon, with the exception of the northern African and Australian fires, when a significant proportion of C<sub>4</sub> plants are being burnt. The largest portion of <sup>13</sup>C-enriched CO enters the atmosphere from December to March from the African equatorial fires. Interestingly, mixing of the fossil fuel-derived CO from ships and the heavier oceanic CO emissions highlights the most navigated ship tracks in the  $\delta^{13}\text{C}(\text{CO})$  map, where the strengths of these sources become comparable.

The average compositions of the majority of NMHCs/VOCs fall in the range of -26 to -24‰ with the exception of isoprene, methanol, propane and butane (Fig. 8). For the latter two, the emission comes predominantly from anthropogenic sources, which are close to -27‰. The isoprene and methanol composition

reflect the significant depletion from the average terrestrial carbon composition. The annual emission dynamics for NMHCs/VOCs generally follows the proportion of the sources, e.g. variations for CH<sub>3</sub>OH and CH<sub>3</sub>COCH<sub>3</sub> are mainly driven by seasonality in biogenic emission. The source dynamics for various NMHCs/VOCs resemble each other, being derived from the same proxies (e.g. burnt carbon in GFED). The uncertainties associated with emission fluxes and corresponding isotope signatures are discussed below in Sect. 3.6.

### 3.5 Pseudo-emission data

For the few long-lived tracers in the current set-up, the pseudo-emission approach is applied by performing the relaxation of the selected species mixing ratios towards the lower boundary conditions (see also Sect. 2 above). The relaxation is handled by the TNUDGE submodel (Kerkweg et al., 2006) and applied at every model time step with typical relaxation times of 3 h for the less reactive compounds (e.g. CH<sub>4</sub>, CO<sub>2</sub>, N<sub>2</sub>O, etc.). The nudging fields are based on the observed mixing ratios from the AGAGE database (Prinn et al., 2000). Amongst the tracers undergoing nudging, CH<sub>4</sub>, CH<sub>3</sub>CCl<sub>3</sub>, CCl<sub>4</sub>, CH<sub>3</sub>Cl, and CO<sub>2</sub> are isotopically separated. For CO<sub>2</sub>, the time series of the zonally averaged composition from the GLOBALVIEW-CO2C13 database (described above in Sect. 3.3.1; see also Fig. 5) was superimposed on the regular CO<sub>2</sub> nudging fields from the EVAL<sub>2</sub> set-up.

Methane (CH<sub>4</sub>) is the major atmospheric in situ source of CO and other reactive carbonaceous species participat-

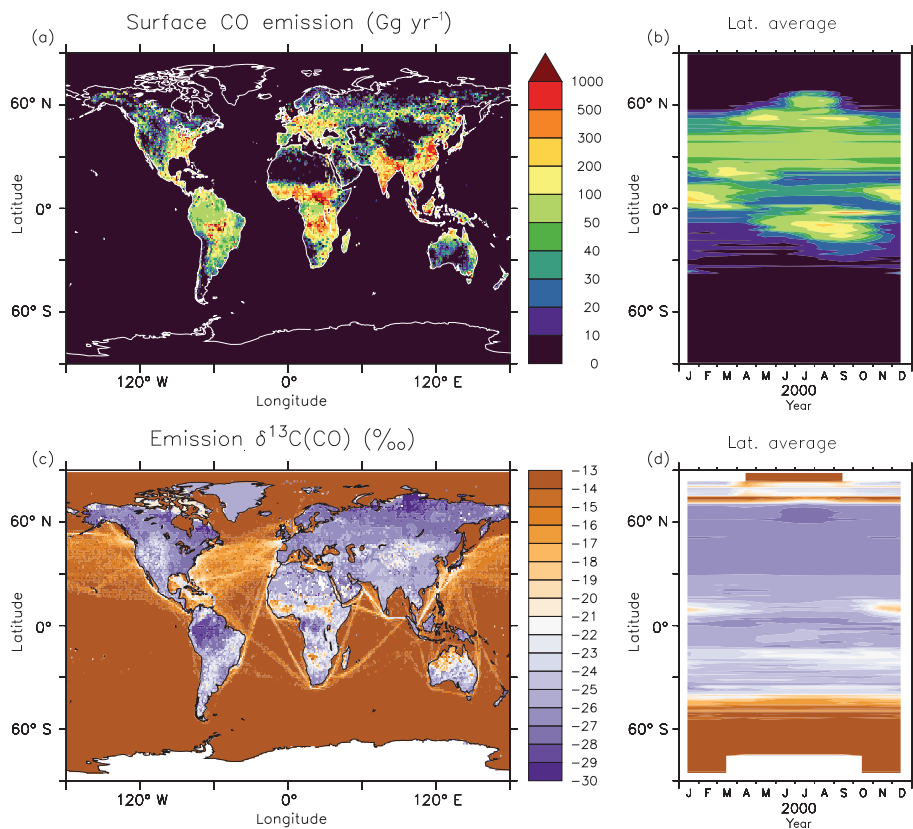


**Figure 7.** (a, c) Annual CO emission from the surface sources (a) and corresponding carbon isotopic composition (c). (b, d) Respective time series of zonal averages for the year 2000 emission with identical colour scale.

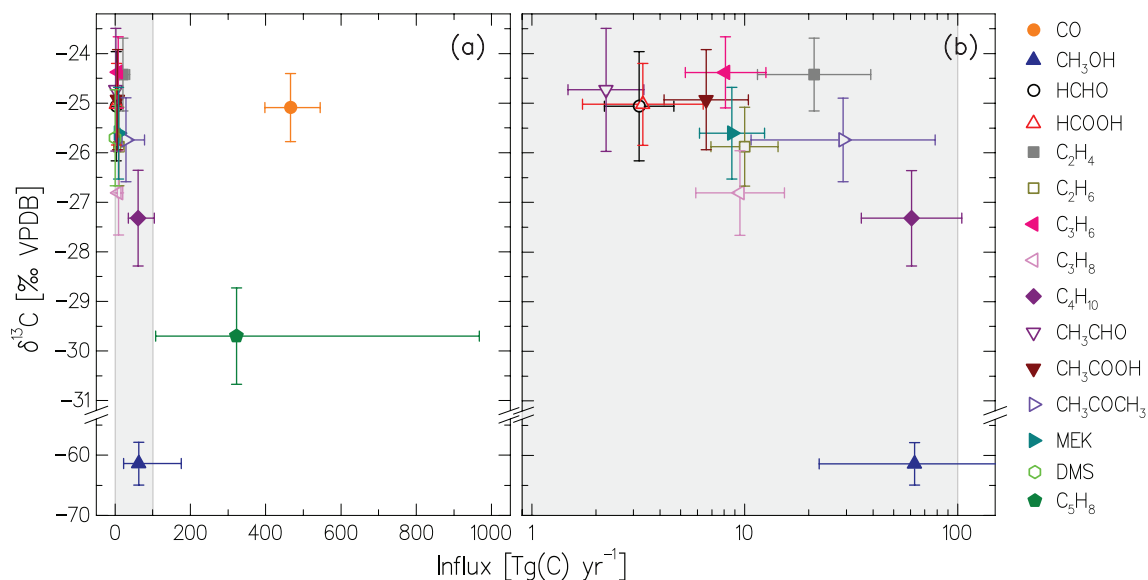


**Figure 8.** (a) Overall annual surface emission isotopic compositions of the carbonaceous compounds. (b) Expanded shaded area in the left panel for the NMHCs/VOCs. The error bars refer to the uncertainty factors from Table 5 and are discussed in Sect. 2.2.

ing in the  $\text{CH}_4 \rightarrow \text{CO}$  oxidation chain. Tropospheric  $\text{CH}_4$  possesses a markedly  $^{13}\text{C}$ -depleted composition, particularly due to the large contribution of the sources associated with the biogenic activity that produces isotopically light methane (see Bréas et al., 2001 and references therein). The average tropospheric  $\delta^{13}\text{C}(\text{CH}_4)$  value of  $-47.3\text{‰}$  (corresponding to the year 2000) ensues from the composition of the surface sources (estimated equilibrated average of  $-51.2\text{‰}$ ) and atmospheric oxidation KIEs, of which the reaction with OH ( $+3.9\text{‰}$ ) is dominant in the troposphere (Saueressig et al., 2001). Since methane is largely abundant and long lived, its signature shows a low variability on top of a weak long-term trend (about  $+0.3\text{‰}$  per decade around the year 2000, Lassey et al., 2000) due to the input of the industrial fossil carbon, and little spatial and temporal variability. Quay et al. (1999) estimated the hemispheric gradient (averages of  $-47.2\text{‰}$  vs.  $-47.4\text{‰}$  for the SH and NH, respectively) and the monthly variation of  $\delta^{13}\text{C}(\text{CH}_4)$  to be both of the order of  $\pm 0.2\text{‰}$ . That is negligible in view of  $\pm 3\text{‰}$  variations in tropospheric  $\delta^{13}\text{C}$  of CO and its large surface sources. Therefore, the constant value of  $-47.2\text{‰}$  is applied to isotopically separate the original nudging fields of  $\text{CH}_4$  in the current set-up.

Of the chlorinated hydrocarbons, the only in situ source of C accounted for in the employed chemical mechanism of MECCA (as of EVAL<sub>2</sub> set-up) is the photolysis of chloromethane yielding  $\text{CH}_3\text{O}_2$ . The remaining chlorinated hydrocarbons contribute only as the in situ sources of Cl; thus their composition is omitted here. The main sources of chloromethane in the atmosphere are to date not clearly identified (Keppler et al., 2005). The estimate of the average global isotopic atmospheric composition is  $\delta^{13}\text{C}(\text{CH}_3\text{Cl}) = -32.6\text{‰}$  (Thompson et al., 2002). This value is used for the pseudo-emission of chloromethane. The contribution of this source to the carbon pool in the atmosphere is low. The estimates of the primary  $\text{CH}_3\text{Cl}$  sink give a global average of  $3.37 \text{ Tg}(\text{CH}_3\text{Cl}) \text{ yr}^{-1}$  through the reaction with OH, equivalent to  $0.8 \text{ Tg}(\text{C}) \text{ yr}^{-1}$  in the oxidised products (methyl peroxy radical).

### 3.6 Uncertainties

In order to calculate the overall emission uncertainties in this study, we account for uncertainties associated with every emission source and its isotope signature, following the methodology described above (Sect. 2.2). The emission magnitudes and uncertainties are expressed in equivalent carbon units to avoid improper counting when isotope ratios are considered. Table 6 lists the uncertainties associated with every emission category/sector. For the fluxes, the uncertainty factors (UF) are quoted, which are commonly reported in emission estimates and refer to a given confidence interval (CI) of emission flux (or typically underlying emission factor) with a given uncertainty probability density distribution (UPDD). For example, the UF of 1.5 may imply that the 95 % CI

of uncertainty spans from  $F/1.5$  to  $1.5 \cdot F$ , or, in percent, from about  $-33$  to  $+50\%$   $F$ , describing a log-normal UPDD around the median value of  $F$ . Exceptionally, the UFs reported for the EDGAR inventory (see Olivier et al., 1999, Table 8) indicate the equivalent span (i.e. Gaussian or any symmetric UPDD) range derived from the largest (i.e. upper end) value, so for the above example it would be  $\pm 50\%$   $F$  around  $F$ . Such treatment is used in our analysis here too (including reporting with the  $\pm$  notation), that is, by selecting the largest (forward) uncertainty ( $F$ ) using the relation

$$\frac{\langle F \rangle}{F} = (u_F - 1), \quad (12)$$

where  $u_F$  is the uncertainty factor. In contrast, uncertainties of isotope signatures are reported plainly in  $\text{‰}$  of  $\delta$ -values assuming normal (Gaussian) UPDD, as the isotopic ratios do not depend on the flux magnitudes.

The uncertainties for some of the signatures have to be derived additionally, referring to the assumptions they are based on. Thus, the uncertainty of the  $\delta^{13}\text{C}$  values of  $\text{C}_3$  and  $\text{C}_4$  plant material composites (i.e. biofuel and biomass burning sources) is derived using Eq. (8) with the  $F_s$  and  $^i R_s$  components substituted by the respective plant material fractions and  $\delta^{13}\text{C}$  signatures. The uncertainties of the latter are inferred as 2 standard deviations of the signature distributions (assumed normal) based on the histogram data of the measured terrestrial compositions (Cerling et al., 1999; Tipple and Pagani, 2007). The isotopic composition variability in  $\text{C}_3$  plants is much larger than that of  $\text{C}_4$ , which is reflected in the resulting uncertainties of  $\langle \delta^{13}\text{C}(\text{C}_3) \rangle = 5.7\text{‰}$  and  $\langle \delta^{13}\text{C}(\text{C}_4) \rangle = 2.5\text{‰}$ . This means that if, for instance, the plant is considered to be of the  $\text{C}_3$  kind, its composition is likely to be found within the range of  $\delta^{13}\text{C}(\text{C}_3) = -(27 \pm 2.9)\text{‰}$ . From the “assumption” point of view, this uncertainty defines the degree of error introduced by prescribing all  $\text{C}_3$  plants to have the composition of the distribution mode of  $-27\text{‰}$ . The errors associated with the plant compositions are the largest in this set-up and they propagate to the final uncertainty mainly via the biofuel category. Interestingly, if one assumes that biofuel plant material comes predominantly from  $\text{C}_4$  plants (e.g. ethanol or biodiesel; see Sect. 3.2), it significantly decreases the overall uncertainty estimate.

An additional calculation is required for those biogenic emissions originating from plants, with signatures that are derived from the leaf discrimination  $\Delta$  and air  $\text{CO}_2$  composition (see Eq. 11). The uncertainty of the latter is of the order of  $0.01\text{‰}$  according to the GLOBALVIEW-CO2C13 data set (see [https://www.esrl.noaa.gov/gmd/ccgg/globalview/gv\\_integration.html](https://www.esrl.noaa.gov/gmd/ccgg/globalview/gv_integration.html) and references therein; here twice that value is assumed). The errors in  $\Delta$  are as large as  $2\text{‰}$ , taking 1 standard deviation of the comparison of the simulated and measured characteristic discriminations for various plant functional types (Scholze et al., 2008). The resulting propagated uncertainty amounts to  $\langle \delta_p \rangle =$

**Table 6.** Uncertainties associated with emission sources and isotopic signatures.

Category	Source	Emission ( $\delta^{13}\text{C}$ signature) uncertainty <sup>a</sup>		
		CO	NMHCs / VOCs	Other <sup>b</sup>
Anthropogenic	Biofuel <sup>c</sup>	2 (4.6‰)	2 (4‰)	–
	Fossil fuel	1.5 (0.3‰) <sup>d</sup>	1.5–2.0 (2‰) <sup>e</sup>	–
	Waste <sup>c</sup>	2 (4‰)	2 (4‰)	–
Biogenic	Land (plants) <sup>f</sup>	3 (1.9‰)	3 (1.9‰)	3 (1.9‰)
	Ocean	2 (3.6‰) <sup>g</sup>	2 (2‰) <sup>h</sup>	–
Biomass burning		1.3 (2‰)	1.3 (2‰) <sup>i</sup>	–
Pseudo-emission <sup>j</sup>	CH <sub>4</sub>	–	–	0.04 % (0.05‰) <sup>k</sup>
	CO <sub>2</sub>	–	–	0.03 % (0.02‰)
	CH <sub>3</sub> Cl	–	–	0.15 % (0.3‰) <sup>m</sup>

<sup>a</sup> Given is the emission uncertainty factors (UFs; see Sect. 3.6) and isotopic signature uncertainty ( $\delta_e$ ) (in parentheses).

<sup>b</sup> Values assumed for biogenic isoprene, terrestrial DMS (plant emitted), and respective pseudo-emitted species.

<sup>c</sup> C<sub>3</sub> / C<sub>4</sub> plant composite, based on  $\langle \delta^{13}\text{C}(\text{C}_3) \rangle = 5.7‰$  and  $\langle \delta^{13}\text{C}(\text{C}_4) \rangle = 2.5‰$  (see text).

<sup>d</sup> From Stevens et al. (1972).

<sup>e</sup> Varies for each species due to the proportion of the fossil fuel (1.5) and industry (2.0) uncertainty factors contribution (Olivier et al., 1999).

<sup>f</sup> The UFs are from Guenther et al. (1995).  $\delta^{13}\text{C}$  uncertainty is derived from  $\langle \delta^{13}\text{C}(\text{CO}_2) \rangle = 0.02‰$  and leaf discrimination uncertainty of  $\Delta = 2‰$ . Exceptionally, methanol  $\langle \delta^{13}\text{C} \rangle = 6.6‰$  is augmented by the uncertainty of plant emission fractionation (Keppler et al., 2004; Yamada et al., 2010,  $\pm 6.3‰$ ; see text).

<sup>g</sup> Following Manning et al. (1997).

<sup>h</sup> Based on variability in  $\delta^{13}\text{C}$  of the marine carbon content from Avery Jr. et al. (2006).

<sup>i</sup> Exceptionally, for methanol  $\langle \delta^{13}\text{C} \rangle = 2.2‰$  is augmented by the uncertainty of BB emission fractionation (Yamada et al., 2009,  $\pm 0.8‰$ ; see text).

<sup>j</sup> Quoted are mixing ratio uncertainties (not uncertainty factors).

<sup>k</sup> Assigned equal to the upper limit of the atmospheric variation.

<sup>m</sup> Error of the mean from Thompson et al. (2002).

1.9‰ (at the average global discrimination of  $\Delta = 17‰$  and  $\delta^{13}\text{C}(\text{CO}_2) = -8‰$ ) and accounts for all plant emissions with the largest UFs at magnitudes of 3 (Guenther et al., 1995). The uncertainty of the biomass burning signatures is set to 2‰ referring to the upper limit of errors in atmospheric  $\delta^{13}\text{C}$  used to validate the C<sub>3</sub>/C<sub>4</sub> burnt vegetation distribution incorporated in the GFEDv2.1 inventory (Still et al., 2003). The UFs for biomass burning emissions are derived from the uncertainties on the estimates for global CO and carbon release in fires by Arellano Jr. et al. (2006) for the April 2000 to March 2001 period obtained using the GFED data (van der Werf et al., 2006).

Employing the methodology described in Sect. 2.2, we derive the resulting overall (combined) uncertainties (listed in Table 5). Essentially high uncertainties are associated with isoprene and plant-dominated emissions of methanol (CH<sub>3</sub>OH), acetone (CH<sub>3</sub>COCH<sub>3</sub>), dimethyl sulfide (DMS) and formic acid (HCOOH). The errors are lower (UFs of 1.5–2) for the species predominantly emitted from the fossil anthropogenic sources. The final uncertainties associated with the isotopic signatures are typically around 1‰, with the biofuel source having a large contribution of (0.3–0.4)‰. The terrestrial emissions are least uncertain, resulting from the lower error in leaf carbon discrimination compared to the uncertainties from C<sub>3</sub>/C<sub>4</sub> plant composites.

Despite the large share of the biofuel sector emissions, the uncertainty of the CO  $\delta^{13}\text{C}$  signature is 0.7‰ due to the compensating input from the fossil fuel sector with a signature of a higher certainty (0.3‰). The final emission strength is defined within  $\pm 17\%$ , yet is a rather large value. When reckoning the surface sources of about 1100 Tg yr<sup>-1</sup> in the global turnover of CO of above 2600 Tg yr<sup>-1</sup> (see the estimates in the following section), the emission uncertainties are expected to propagate in the model result errors with at most  $\pm 30\%$  in CO mixing ratios and  $\pm 1.3‰$  in  $\delta^{13}\text{C}(\text{CO})$ . To estimate the uncertainties associated with the in situ-produced CO, the emission/isotope signature uncertainties of the respective NMHC/VOC sources should be used as the proxies accordingly.

## 4 Discussion

### 4.1 $^{13}\text{CO}/^{12}\text{CO}$ emissions

Table 7 lists our resulting  $^{13}\text{C} / ^{12}\text{C}$ -resolved CO emission inventory compared with the estimates available from previous studies. Notably, the bottom-up estimates (including the a priori set-ups for the inverse modelling studies) integrate more  $^{13}\text{C}$ -depleted fluxes and vary less significantly between different studies, i.e. within  $-35$  to  $-33‰$  in  $\delta^{13}\text{C}$ . The ear-

**Table 7.** Tropospheric CO sources and their isotopic composition from the present and previous studies.

Study	SW89	B99 <sup>a</sup>	M97 <sup>a, b, c</sup>	B00 <sup>a, b, c</sup>	E04 <sup>a, d</sup>	Eval <sub>2</sub> <sup>a, d</sup>
Model	–	–	GFDL (2D)	TM2	MOZART2	EMAC
Emission inventories <sup>e</sup>	1971	1972–1998	1987–1995	1987 <sup>+</sup>	1997–1999	2000 <sup>+</sup>
CH <sub>4</sub> oxidation	(–55) <sup>f</sup>	400–1000 (–52.6)	624 (–52.6)	795 (–51.1)	1022 (–51)	834 (–51.2)
NMHC oxidation	(–32.3) <sup>f</sup>	200–600 (–32.2)	403 (–29.3)	607 (–23.9)	453 (–30)	579 (–26.1) <sup>g</sup>
Fossil fuel/ biofuel usage	480 (–27.5)	300–550 (–27.5)	595 (–27)	641 (–26.7)	361 (–27)/ 306 (–25)	272 (–27.4)/ 285 (–25)
Biomass burning	1195 (–24)	300–700 (–24.5)	909 (–21)	768 (–20)	570 (–21.8)	434 (–24.1)
Biogenic/ oceans		60–160 (–)/ 20–200 (–13.5)	–/ 57 (–13.5)	–/ 49 (5.1)	158 (–32)/ 20 (–12)	102 (–25.7)/ 13 (–13.5)
Photochemical sources	1100–1250 (–38.4) <sup>f</sup>	1265 (–33.5) <sup>h</sup>	1027 (–43.4)	1402 (–39.3)	1475 (–44.6)	1414 (–40.9) <sup>g</sup>
Uncertainty	±125 (±1.7)	±180 (±3.7)	±182 (±3.5)	±127 (±2.5)	–	±420 (±4.4)
<b>Surface sources</b>	<b>1550–1700 (–25)</b>	<b>1285 (–24.8)<sup>h</sup></b>	<b>1561 (–23)</b>	<b>1458 (–22.1)</b>	<b>1415 (–24.8)</b>	<b>1086 (–25.2)</b>
<b>Uncertainty</b>	<b>±125 (±1.7)</b>	<b>±238 (±1.4)</b>	<b>±207 (±2.4)</b>	<b>±125 (±1.8)</b>	–	<b>±194 (±0.7)</b>
Total sources	2800 (–30.3)	2550 (–34.9)	2588 (–31.1)	2860 (–30.5)	2890 (–34.9)	2525 (–34.1) <sup>g</sup>
Overall uncertainty	±250 (±2)	±216 (±1.4)	±389 (±3.4)	±252 (±2.4)	–	±462 (±1.6)

Notes: the source terms/uncertainties are given in  $[\text{Tg}(\text{CO})\text{yr}^{-1}]$  with the corresponding  $\delta^{13}\text{C}$  composition in [‰ V-PDB] in parentheses. Values are the tropospheric averages; boldface emphasises the total surface emission term scrutinised in this study. Abbreviations refer to SW89: Stevens and Wagner (1989); M97: Manning et al. (1997) (case2); B99: Brenninkmeijer et al. (1999); B00: Bergamaschi et al. (2000) (scenario S2); E04: Emmons et al. (2004); EVAL<sub>2</sub>: this study (see Sects. 1, 2).

<sup>a</sup> A bottom-up estimate (for the inverse modelling studies, the a priori set-up).

<sup>b</sup> An inversion technique to improve the emission strengths/isotope signatures is employed.

<sup>c</sup> A simplified chemistry scheme (no intermediates in the  $\text{CH}_4 \rightarrow \text{CO}$  chain, no NMHC chemistry) is used.

<sup>d</sup> A detailed chemistry scheme (e.g.  $\text{CH}_4$  and NMHC chemistry with intermediates and removal processes) is used.

<sup>e</sup> The year(s) the aggregate of the emission inventories correspond closest to; the plus signs indicate that the transient biomass burning inventory was used, with the listed year referring to the anthropogenic emissions revision.

<sup>f</sup> The authors assume a too high NMHC:  $\text{CH}_4$  source fluxes partitioning of 5.5 : 1 based on then limited information on sources O isotope composition. The  $^{13}\text{C}$  mass-balance and photochemical source is reanalysed here in light of current knowledge on the  $\delta^{18}\text{O}$  signatures of CO sources (see, e.g. B99).

<sup>g</sup> Upper limit, assuming  $\delta^{13}\text{C}$  of emitted  $\text{CH}_3\text{OH}$  being similar to that of other NMHCs/VOCs (about  $-(26 \pm 1)\text{‰}$ ).

<sup>h</sup> The total signature results from the respective source terms averaged within the given limits.

liest top-down estimate of  $-30.3\text{‰}$  given by Stevens and Wagner (1989) (hereinafter denoted SW89) is rather uncertain about the individual sources apportioning, being derived using the average atmospheric  $\delta^{13}\text{C}(\text{CO})$  observed by that time corrected for the average tropospheric  $^{13}\text{C}$ CO enrichment (reckoned to be  $+3\text{‰}$  due to the KIE escorting the removal of CO by OH). Similar to SW89, the a posteriori estimates from the more elaborate inverse modelling studies favour the overall CO source  $\delta^{13}\text{C}$  of  $-31.1$  to  $-30.5\text{‰}$  resulting from the larger  $^{13}\text{C}$ -enriched surface influx and reduced methane oxidation source shares. The difference between the bottom-up and top-down estimates of the primary sources is  $3\text{--}4\text{‰}$ , which, if one assumes the CO yield from  $\text{CH}_4$  oxidation being nearly unity, causes an even larger disparity in the estimates of the average  $\delta^{13}\text{C}$  of the non- $\text{CH}_4$  CO sources. Thus, from Manning et al. (1997) (M97) and Bergamaschi et al. (2000) (B00) these should be  $-21.3\text{‰}$ , whereas for the other studies the non-methane CO source signature is much lower, e.g.  $-26.1\text{‰}$  in Emmons et al. (2004) (E04) and  $-25.2\text{‰}$  (this study, EVAL<sub>2</sub>). From the CO budget considerations of Brenninkmeijer et al. (1999) (B99) one derives similar  $^{13}\text{C}$ -depleted source composition when superimposing the respective  $\delta^{13}\text{C}$  values from the literature on their reported emission strengths.

Figure 9b details the global CO source by category from the previous and current isotope-enabled studies. Neither bottom-up nor top-down estimates show correlated tendencies, suggesting the overall CO budget is uncertain within at least  $\pm 200 \text{ Tg}(\text{CO})\text{yr}^{-1}$ . One infers a similar estimate of about  $2700 \pm 280 \text{ Tg}(\text{CO})\text{yr}^{-1}$  from the results of the ensemble of the inverse modelling approaches summarised by Duncan et al. (2007), narrowed down to  $2500 \pm 185 \text{ Tg}(\text{CO})\text{yr}^{-1}$  for the year 2000 (see references therein; the ensemble average of  $\pm 1$  standard deviation is quoted). The large variation of  $2500\text{--}2900 \text{ Tg}(\text{CO})\text{yr}^{-1}$  of these estimates (quoted range refers to the year 2000 or to the interannual averages conferred by the studies regarded) is generally attributed to the differences in the implementation of inverted surface emission strengths. Regarding the variation range of individual CO sources between the studies, the largest spread of around  $280 \text{ Tg}(\text{CO})\text{yr}^{-1}$  (or equivalent 50 % of its average value) is attributed to the biomass burning (BB) source. The most ambiguous biogenic source (including oceanic emission) varies within around 70 % of its average, or  $90 \text{ Tg}(\text{CO})\text{yr}^{-1}$ , but is nonetheless least influential in the aggregate emission composition. The moderately uncertain fossil fuel/biofuel (FF/BF) and VOCs oxidation sources range within about 25 and 30 % ( $170$  and  $150 \text{ Tg}(\text{CO})\text{yr}^{-1}$ ). Disregarding the rather low a posteriori estimates of M97 and B00, the

methane source of CO appears the most certain one, ranging only within 15 % or roughly  $110 \text{ Tg}(\text{CO}) \text{ yr}^{-1}$  around its average value.

Amongst the studies regarded here, the a priori and bottom-up-derived sources sum up to about  $2900 \text{ Tg}(\text{CO}) \text{ yr}^{-1}$ ; i.e. they lie at the upper end of the range quoted above. The a posteriori sources in B00 are generally reduced at the expense of the smaller  $\text{CH}_4$  source. In contrast, M97 compensates the decrease in the total photochemically produced CO by surface sources, thus keeping the final emission strengths close to the initial guess. Note that these two studies also infer the largest BB emission sources exceeding the interstudy average by a factor of two-thirds and one-third. A significantly lower CO budget in M97 is most probably a drawback of using the fairly limited observational data from the extratropical SH, where the inversion results are less sensitive to the NH sources, including their underestimation. Comparably low CO emissions for EMAC are derived here, which, when applied, are likely to result in systematically low simulated NH high-latitude CO mixing ratios, particularly in winter. A similar feature was observed in the previous studies with EMAC (Pozzer et al., 2007; their set-up is being closely followed here; see Sect. 2), as well as in other employed models/inventories (e.g. B00 and E04; see also Stein et al., 2014, and references therein). Stein et al. (2014) show that a more detailed representation of the strength and seasonality of CO dry deposition fluxes and traffic emissions in Europe and North America leads to more adequately reproduced NH CO mixing ratios. It is noteworthy that their hypothesis that the missing traffic CO is due to emission inventories not accounting for cold-start engine conditions should be verifiable through  $^{18}\text{O} / ^{16}\text{O}$  ratio of emitted CO: the latter (but unfortunately not  $^{13}\text{C} / ^{12}\text{C}$  ratio) differ substantially between the BB and FF sources (see Kato et al., 1999a, also Sect. 3.1). Nevertheless, it is clear that strengths and spatial distribution of the missing CO sources shall receive a more thorough quantification through the isotope-resolved inventories, which we undertake in subsequent studies.

In addition to the comparison of the CO source strengths, Fig. 9a elucidates individual contributions of every source term to the  $\delta^{13}\text{C}$  value of total emitted CO in the isotope-inclusive budget. The source terms (bars) are calculated as the products ( $f_s \cdot \delta_s$ ), where  $f_s$  is the fractional contribution and  $\delta_s$  is the  $\delta^{13}\text{C}$  of a particular CO source. This way one grasps the integration of individual inputs enriching/depleting the final composition (with respect to the reference ratio of 0‰), which also highlights the interstudy variation of each source input. Because the majority of the CO sources are depleted, the calculated contributions are always negative, with an exception of the minute term of +0.1‰ in B00 from the oceanic source with a corresponding  $\delta_s = +5.1‰$  (added up to the biogenic category). Due to the appreciably  $^{13}\text{C}$ -depleted composition of methane

(−51.2‰), the overall composition is highly sensitive to the  $\text{CH}_4$  source input, with clearly smaller contributions in M97 and B00. In contrast, the variation in the total surface source input to  $\delta^{13}\text{C}$  is rather low, as opposed to the variation in respective fluxes.

Coherent adjustments to the source composition in the a posteriori estimates are given by the inverse studies, however they remain within the uncertainty ranges of the a priori guesses (note that these are based on different isotope signatures as well, not listed in Table 7). Despite the improved uncertainties for almost each individual source category, the combined (either surface or total) a posteriori source estimates' uncertainties are essentially larger than those of the prior guesses, owing to the correlated nature of the inverted components (see Sect. 2.2 for elucidation). Thus, posterior combined uncertainties increase by a factor of 1.3–1.7 (fluxes) and 2.4–3.1 (flux  $\delta^{13}\text{C}$  values) with respect to those of the independent priors. An exception is the reduction of uncertainty in the overall surface CO flux (factor of 0.8) but not its  $\delta^{13}\text{C}$  value (increase, factor of 1.2) in B00, which, however, does not reduce the final overall uncertainty.

Furthermore, on a global scale the posterior repartitioning of the non-methane sources is virtually ineffective in M97: an increase of +2.7‰ in  $\delta_s$  of the VOC oxidation source counterbalances the sufficiently larger BB source in the optimised emissions, hence the increase in tropospheric  $\delta^{13}\text{C}(\text{CO})$  is merely promoted by adjusting the  $\text{CH}_4$  source. The reduction of the methane component in B00 is less marginal, whilst the non-methane sources also deplete the final  $\delta^{13}\text{C}(\text{CO})$  less, being enriched by a similar adjustment of the VOC signature by +2.5‰. Despite the fact that the  $\text{CH}_4$  source strength inferred by B00 is comparable to the majority of the estimates presented in Fig. 9b, its relative contribution to the overall CO is diminished by a larger fraction of the other sources, which is a direct consequence of the reduced CO yield (0.86) from  $\text{CH}_4$ . The remaining studies suggest almost complete conversion of the  $\text{CH}_4 + \text{OH}$  source to CO, and by this confine the overall source  $\delta^{13}\text{C}$  to the −35 to −33‰ range. The results of the inversion studies (including the top-down estimate of SW89) importantly retain the expected tropospheric average of above −28‰ assimilated to a considerable extent from the observational data at the surface. Regarding the bottom-up estimates, it becomes clear that the CO + OH sink fractionation, when assumed to be about +3‰, is capable of bringing the tropospheric  $\delta^{13}\text{C}(\text{CO})$  value at most to −30.5‰, which is a perceptibly underestimated  $^{13}\text{CO} / ^{12}\text{CO}$  tropospheric ratio.

#### 4.2 $^{13}\text{C} / ^{12}\text{C}$ ratios of NMHCs/VOCs emission

Only one  $^{13}\text{C}$ -inclusive global-scale emission estimate for ethane is available to date for comparison with the NMHC/VOC emissions derived here. Using two 3-D chemical transport models (CTM), Stein and Rudolph (2007) (hereinafter SR07) evaluate two emission sets based on the

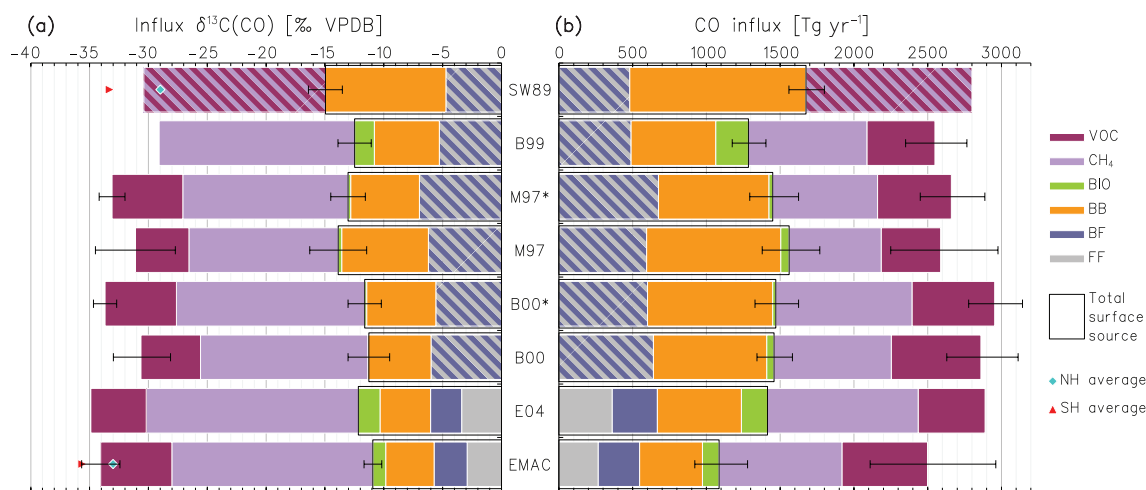


**Figure 9.** Estimates of the tropospheric CO sources and their contribution to the overall source isotope composition from previous and the present studies (refers to Table 7). Abbreviations refer to: SW89: Stevens and Wagner (1989); M97: Manning et al. (1997) (case 2); B99: Brenninkmeijer et al. (1999); B00: Bergamaschi et al. (2000) (scenario S2); E04: Emmons et al. (2004); EMAC: this study, set-up based on EVAL<sub>2</sub>, year 2000 (see text, Sect. 2). Asterisks denote a priori estimates of the corresponding inverse modelling studies. Note: blue-grey hatched bars denote the aggregate of industrial emissions (FF and BF sources are not distinguished); SW89 report the total of photochemical sources only (light blue-violet hatched bars, respectively). Black frames denote the values for the total surface component. **(b)** Source terms by category. **(a)** Individual contribution of each source category to the overall source  $\delta^{13}\text{C}(\text{CO})$ , calculated as a product of the share in total emission and respective source  $\delta^{13}\text{C}$  average. Symbols denote the hemispheric tropospheric averages, where available.

GEIA/EDGAR inventories (detailed in Sect. 2), which differ in inclusion of the biofuel, biogenic and oceanic sources. By integrating the same literature sources (listed in Sect. 3), the authors use slightly different assumptions on the isotope composition of emitted  $\text{C}_2\text{H}_6$ , namely  $\delta^{13}\text{C}$  signatures of the  $\text{C}_4$  plant carbon of  $-13\text{‰}$ , fossil-fuel carbon of  $-26\text{‰}$  and gas production and transmission of  $-32\text{‰}$ , respectively. Furthermore, anthropogenic emission fluxes in SR07 are based on the previous version (2.0) of the EDGAR inventory. Being optimised in simulations with CTMs, emissions in SR07 offer more independent comparison against the current results based on the newer version (3.2) of EDGAR (see Sect. 3.1).

Both estimates of  $\text{C}_2\text{H}_6$  emission fluxes by SR07 are lower than, but within the uncertainty range of the estimate reckoned here, i.e. 8.2 in MOZART CTM emissions (MOZ) and 9.57 in GISS CTM emissions (GISS) compared to  $12.48 \pm 5.49 \text{ Tg}(\text{C}_2\text{H}_6) \text{ yr}^{-1}$  in EMAC, respectively. The  $\delta^{13}\text{C}$  of total emitted ethane ( $-28.5\text{‰}$ ) in MOZ is virtually identical to the value derived here (see Table 5). However it is composed of very different relative inputs (that is, the  $f_s \cdot \delta_s$  terms; see previous section). Their shares (FF + BF : BB : biogenic) are lighter in the anthropogenic component in MOZ ( $-13.8\text{‰} : -9.6\text{‰} : -2.4\text{‰}$ ) vs. those in EMAC ( $-19.6\text{‰} : -5.3\text{‰} : -0.9\text{‰}$ , respectively). Projecting the  $\delta^{13}\text{C}$  signatures of MOZ onto the GISS fluxes yields a slightly lower overall emission  $\delta^{13}\text{C}$  of  $-26.6\text{‰}$  ( $-19.8\text{‰} : -6.8\text{‰}$ ; no value), which is still on the lower end of  $-(25.9 \pm 0.8\text{‰})$  obtained in EMAC. A similar pro-

jection of the emission  $\delta^{13}\text{C}$  signatures used by SR07 onto the emission fluxes in EMAC, and vice versa, yields the large span of the overall emission  $\delta^{13}\text{C}$  value of  $-(18.6\text{--}22.4)\text{‰}$ , which suggests that the  $^{13}\text{C}$ -resolved  $\text{C}_2\text{H}_6$  emission inventories should be rather sensitive to the ratio of anthropogenic and biogenic inputs. In this respect, the results obtained here for EMAC reconcile both the underestimated anthropogenic sources highlighted by SR07 and their (top-down) estimate of the global ethane  $\delta^{13}\text{C}$  signature.

SR07 do not provide a detailed uncertainty analysis for their emission estimates. Nonetheless, we attempt to derive these by applying the analysis and uncertainty factors reckoned for EMAC here (see Sect. 3.6, also Table 6), since similar emission categories and the same literature sources are used. Thus derived global emission flux uncertainties in SR07 are of  $\pm 29\%$  and  $\pm 32\%$  in MOZ and GISS, respectively, and are noticeably lower than  $\pm 44\%$  in EMAC, mostly owing to the different treatment of the BF sources (these are assumed by SR07 known with greater certainty, i.e. that of the FF sources). In contrast, the overall  $\delta^{13}\text{C}$  signature uncertainties are only slightly improved with respect to those in EMAC, viz. to  $\pm 0.7$  and  $\pm 0.6\text{‰}$  in MOZ and GISS, respectively. We may therefore conclude that all three estimates considered here agree in strength and isotope ratio of the global ethane emission flux.

## 5 Concluding remarks

In this study, we attempt to deliver a comprehensive up to date review on the  $^{13}\text{C}/^{12}\text{C}$  ratios of emission sources of atmospheric CO and other reactive carbonaceous compounds. As a consistent starting point for the isotope extension, we choose the evaluated emission set-up of the EMAC model (EVAL<sub>2</sub>; see Sect. 2). The latter does not employ the most recent versions of some inventories (e.g. EDGAR). However, we believe the information on proxies and the uncertainty analysis offered here should suffice and enable one to perform a complete isotope extension of any desired up-to-date inventory in a fashion similar to that presented here.

Compiling the isotope-inclusive emission inventory immediately highlights several peculiarities of the  $^{13}\text{CO}$  budget in comparison with previous studies:

- First, we corroborate that the bottom-up and top-down estimates disagree on the overall surface-emitted CO isotope signature, with the top-down approaches reckoned to be (2–3)% heavier in  $\delta^{13}\text{C}$ . This discrepancy is larger than the associated uncertainties in all studies regarded here (an exception is the a posteriori estimate of M97) and calls further for clarification.
- Second, we note that our estimate has a substantially lower uncertainty ( $\pm 0.7\%$ ) associated with the total surface emission term. Furthermore, accurate use of probabilistic calculus renders the a posteriori global estimates of the inverse modelling studies generally less certain than their a priori guesses (in the case of correlated estimates). This may leave bottom-up approaches favourable, as an increase in boundary condition data fed into inverse models does not necessarily reduce posterior uncertainties to adequate levels (cf. uncertainties in M97 and B00 with the latter utilising a substantially larger set of observational data).
- Third, isotope mass-balancing of the CO sources is very sensitive to the input of  $^{13}\text{C}$ -depleted carbon from the  $\text{CH}_4$  oxidation source (see Fig. 9 and Table 7), with the key question being the tropospheric yield of CO from methane oxidation. Although the production of CO from  $^{13}\text{C}$ -depleted methanol is minor compared to the  $\text{CH}_4$  oxidation source, its strong depletion may aggravate this issue. Only E04 have explicitly accounted for  $\text{CH}_3\text{OH}$  in their model set-up with average emission  $\delta^{13}\text{C}$  of  $-30\%$  compared to  $-(61.4 \pm 3.6)\%$  in the current set-up with EMAC.

The aspects outlined above highlight disagreements between the bottom-up and top-down approaches on the  $^{13}\text{CO}$  atmospheric budget, which are not yet reconciled. Perhaps, a hybrid iterative approach consisting of inverse modelling steps (performing optimisation of the emission fluxes only), followed by forward modelling steps (applying less uncertain bottom-up isotope signatures) could offer an efficient solution to this problem.

At last, the comparison of our results with the study by SR07 on isotope-resolved ethane emissions provides evidence that isotope ratio information may bring deeper insights into studies dealing with NMHCs/VOCs as well, even at the stage of compiling the emission inventories, e.g. comparing their versions. We therefore hope that current results will bolster the community for further efforts in this little-explored area of atmospheric isotope composition modelling field.

*Data availability.* We provide the surface emission fluxes estimated here in the supplementary data available at <https://doi.org/10.1594/PANGAEA.877301> (Gromov et al., 2017). The offline emissions for the anthropogenic, biogenic and biomass burning sources are encapsulated in separate NetCDF files. The online calculated emissions (e.g.  $\text{C}_5\text{H}_8$ ) and pseudo-emission (nudging) data are not included.

**Appendix A: On the choice of the  $^{13}\text{C}$   $R_{\text{st}}$  value**

We note that the value of  $^{13}\text{C}$   $R_{\text{st}}$  from Craig (1957) has been nominally outdated since the last redetermination of the carbon isotope ratio of the NBS 19 reference material used to define the hypothetical V-PDB scale introduced after the former PDB primary material was exhausted (see Chapter 40 in de Groot, 2004; Zhang et al., 1990; Brand et al., 2010). Owing to the differences between the former (i.e. assigned from PDB) and revised scales, a change in isotope composition corresponding to 1 ‰ in  $\delta^{13}\text{C}$  on the PDB scale is about 0.001176 ‰ larger on the V-PDB scale, which implies different ex-post facto absolute abundances derived using the same  $\delta^{13}\text{C}$  values reported. The resulting emission  $\delta^{13}\text{C}$  signatures presented here are sensitive to the choice of these standards, since absolute emission fluxes are defined through them. Nonetheless, errors introduced by adopting outdated values are negligible compared to uncertainties introduced by the other factors, e.g. laboratory/model estimates of the emission strengths and signatures (see Sect. 3.6, also Table 6).

*Competing interests.* The authors declare that they have no conflict of interest.

*Acknowledgements.* Authors are grateful to Alan Goldstein (UC Berkeley), Elena Popa (IMAU Utrecht) and Taku Umezawa (NIES Tsukuba) for fruitful discussions on CO and trace gas emissions and their isotope composition particularities. Andrea Pozzer (MPI-C Mainz) is acknowledged for the great help with the biogenic emissions in EMAC. We appreciate the expertise on standard isotope ratios application from Sergey Assonov (IAEA Environmental Labs Vienna), the erroneous formulation pointed out by Franziska Frank (DLR Oberpfaffenhofen) and important comments on the  $\text{CH}_3\text{Cl}$  isotope composition by Frank Keppler (GEOW Heidelberg). Last but not least, we are indebted to two anonymous referees whose expertise and valuable input led to substantial improvement of this manuscript.

The article processing charges for this open-access publication were covered by the Max Planck Society.

Edited by: Astrid Kiendler-Scharr

Reviewed by: two anonymous referees

## References

- Affek, H. P. and Yakir, D.: Natural Abundance Carbon Isotope Composition of Isoprene Reflects Incomplete Coupling between Isoprene Synthesis and Photosynthetic Carbon Flow, *Plant Physiol.*, 131, 1727–1736, <https://doi.org/10.1104/pp.102.012294>, 2003.
- Andreae, M. O. and Merlet, P.: Emission of trace gases and aerosols from biomass burning, *Global Biogeochem. Cy.*, 15, 955–966, <https://doi.org/10.1029/2000gb001382>, 2001.
- Arellano Jr., A. F., Kasibhatla, P. S., Giglio, L., van der Werf, G. R., Randerson, J. T., and Collatz, G. J.: Time-dependent inversion estimates of global biomass-burning CO emissions using Measurement of Pollution in the Troposphere (MOPITT) measurements, *J. Geophys. Res.*, 111, D09303, <https://doi.org/10.1029/2005jd006613>, 2006.
- Avery Jr., G. B., Willey, J. D., and Kieber, R. J.: Carbon isotopic characterization of dissolved organic carbon in rainwater: Terrestrial and marine influences, *Atmos. Environ.*, 40, 7539–7545, <https://doi.org/10.1016/j.atmosenv.2006.07.014>, 2006.
- Bates, T. S., Kelly, K. C., Johnson, J. E., and Gammon, R. H.: Regional and seasonal variations in the flux of oceanic carbon monoxide to the atmosphere, *J. Geophys. Res.*, 100, 23093–23101, <https://doi.org/10.1029/95jd02737>, 1995.
- Bergamaschi, P., Hein, R., Brenninkmeijer, C. A. M., and Crutzen, P. J.: Inverse modeling of the global CO cycle: 2. Inversion of  $^{13}\text{C} / ^{12}\text{C}$  and  $^{18}\text{O} / ^{16}\text{O}$  isotope ratios, *J. Geophys. Res.*, 105, 1929–1945, <https://doi.org/10.1029/1999jd900819>, 2000.
- Boutton, T. W.: Stable carbon isotope ratios of natural materials: II. Atmospheric, terrestrial, marine, and freshwater environments, in: *Carbon Isotope Techniques*, edited by: Coleman, D. and Fry, B., Elsevier, New York, 173–185, 1991.
- Brand, W. A., Assonov, S. S., and Coplen, T. B.: Correction for the  $^{17}\text{O}$  interference in  $\delta^{13}\text{C}$  measurements when analyzing  $\text{CO}_2$  with stable isotope mass spectrometry (IU-PAC Technical Report), *Pure Appl. Chem.*, 82, 1719–1733, <https://doi.org/10.1351/pac-rep-09-01-05>, 2010.
- Bréas, O., Guillou, C., Reniero, F., and Wada, E.: The global methane cycle: isotopes and mixing ratios, sources and sinks, *Isot. Environ. Health S.*, 37, 257–379, <https://doi.org/10.1080/10256010108033302>, 2001.
- Brenninkmeijer, C. A. M.: Measurement of the abundance of  $^{14}\text{CO}$  in the atmosphere and the  $^{13}\text{C} / ^{12}\text{C}$  and  $^{18}\text{O} / ^{16}\text{O}$  ratio of atmospheric CO with applications in New Zealand and Antarctica, *J. Geophys. Res.*, 98, 10595–10614, <https://doi.org/10.1029/93JD00587>, 1993.
- Brenninkmeijer, C. A. M., Röckmann, T., Bräunlich, M., Jöckel, P., and Bergamaschi, P.: Review of progress in isotope studies of atmospheric carbon monoxide, *Chemosphere – Global Change Science*, 1, 33–52, [https://doi.org/10.1016/S1465-9972\(99\)00018-5](https://doi.org/10.1016/S1465-9972(99)00018-5), 1999.
- Brenninkmeijer, C. A. M., Janssen, C., Kaiser, J., Röckmann, T., Rhee, T. S., and Assonov, S. S.: Isotope effects in the chemistry of atmospheric trace compounds, *Chem. Rev.*, 103, 5125–5161, <https://doi.org/10.1021/Cr020644k>, 2003.
- Cerling, T. E., Harris, J. M., and Leakey, M. G.: Browsing and Grazing in Elephants: The Isotope Record of Modern and Fossil Proboscideans, *Oecologia*, 120, 364–374, <https://doi.org/10.1007/s004420050869>, 1999.
- Conny, J. M.: The isotopic characterization of carbon monoxide in the troposphere, *Atmos. Environ.*, 32, 2669–2683, [https://doi.org/10.1016/S1352-2310\(97\)00398-1](https://doi.org/10.1016/S1352-2310(97)00398-1), 1998.
- Conny, J. M. and Currie, L. A.: The isotopic characterization of methane, non-methane hydrocarbons and formaldehyde in the troposphere, *Atmos. Environ.*, 30, 621–638, [https://doi.org/10.1016/1352-2310\(95\)00305-3](https://doi.org/10.1016/1352-2310(95)00305-3), 1996.
- Craig, H.: Isotopic standards for carbon and oxygen and correction factors for mass-spectrometric analysis of carbon dioxide, *Geochim. Cosmochim. Ac.*, 12, 133–149, [https://doi.org/10.1016/0016-7037\(57\)90024-8](https://doi.org/10.1016/0016-7037(57)90024-8), 1957.
- Criss, R. E.: *Principles of Stable Isotope Distribution*, Oxford University Press, New York, 264 pp., 1999.
- Czapiewski, K. V., Czuba, E., Huang, L., Ernst, D., Norman, A. L., Koppmann, R., and Rudolph, J.: Isotopic composition of non-methane hydrocarbons in emissions from biomass burning, *J. Atmos. Chem.*, 43, 45–60, <https://doi.org/10.1023/a:1016105030624>, 2002.
- D’Agostini, G.: *Asymmetric Uncertainties: Sources, Treatment and Potential Dangers*, eprint arXiv:physics/0403086, 2004.
- Dawson, T. E., Mambelli, S., Plamboeck, A. H., Templer, P. H., and Tu, K. P.: Stable Isotopes in Plant Ecology, *Annu. Rev. Ecol. Syst.*, 33, 507–559, <https://doi.org/10.1146/annurev.ecolsys.33.020602.095451>, 2002.
- de Groot, P. A.: *Handbook of Stable Isotope Analytical Techniques*, Elsevier, 1234 pp., 2004.
- Demirbas, A.: Biofuels sources, biofuel policy, biofuel economy and global biofuel projections, *Energ. Convers. Manage.*, 49, 2106–2116, <https://doi.org/10.1016/j.enconman.2008.02.020>, 2008.
- Demirbas, A.: Political, economic and environmental impacts of biofuels: A review, *Appl. Energ.*, 86, S108–S117, <https://doi.org/10.1016/j.apenergy.2009.04.036>, 2009.

- Drosg, M.: Dealing with Uncertainties: A Guide to Error Analysis, Springer, 235 pp., 2009.
- Dube, O. P.: Linking fire and climate: interactions with land use, vegetation, and soil, *Current Opinion in Environmental Sustainability*, 1, 161–169, <https://doi.org/10.1016/j.cosust.2009.10.008>, 2009.
- Duncan, B. N., Logan, J. A., Bey, I., Megretskaya, I. A., Yantosca, R. M., Novelli, P. C., Jones, N. B., and Rinsland, C. P.: Global budget of CO, 1988–1997: Source estimates and validation with a global model, *J. Geophys. Res.*, 112, D22301, <https://doi.org/10.1029/2007jd008459>, 2007.
- Emmons, L. K., Hess, P., Lamarque, J. F., Orlando, J. J., Pétron, G., Mak, J., Randerson, J., and Granier, C.: Improving CO Emissions using  $^{13}\text{C}/^{12}\text{C}$  Fractions in Observations and MOZART, 8th International Global Atmospheric Chemistry Conference (IGAC 2004), Christchurch, New Zealand, 4–9 September 2004.
- Enting, I. G.: Inverse problems in atmospheric constituent transport, Cambridge Atmospheric and Space Science Series, Cambridge University Press, New York, 2002.
- Farquhar, G. D., Ehleringer, J. R., and Hubick, K. T.: Carbon Isotope Discrimination and Photosynthesis, *Annu. Rev. Plant Phys.*, 40, 503–537, <https://doi.org/10.1146/annurev.pp.40.060189.002443>, 1989.
- Ganzeveld, L. N., Lelieveld, J., Dentener, F. J., Krol, M. C., Bouwman, A. J., and Roelofs, G. J.: Global soil-biogenic  $\text{NO}_x$  emissions and the role of canopy processes, *J. Geophys. Res.*, 107, ACH-9-1–ACH-9-17, <https://doi.org/10.1029/2001JD001289>, 2002.
- Gensch, I., Kiendler-Scharr, A., and Rudolph, J.: Isotope ratio studies of atmospheric organic compounds: Principles, methods, applications and potential, *Int. J. Mass Spectrom.*, 365–366, 206–221, <https://doi.org/10.1016/j.ijms.2014.02.004>, 2014.
- Giebel, B. M., Swart, P. K., and Riemer, D. D.:  $\delta^{13}\text{C}$  Stable Isotope Analysis of Atmospheric Oxygenated Volatile Organic Compounds by Gas Chromatography-Isotope Ratio Mass Spectrometry, *Anal. Chem.*, 82, 6797–6806, <https://doi.org/10.1021/ac1007442>, 2010.
- GLOBALVIEW-CO2C13: Cooperative Atmospheric Data Integration Project –  $\delta^{13}\text{C}$  of Carbon Dioxide, CD-ROM, NOAA ESRL, Boulder, Colorado, available at: [https://www.esrl.noaa.gov/gmd/ccgg/globalview/co2c13/co2c13\\_intro.html](https://www.esrl.noaa.gov/gmd/ccgg/globalview/co2c13/co2c13_intro.html) (last access: March 2015), 2009.
- Goldstein, A. H. and Shaw, S. L.: Isotopes of Volatile Organic Compounds: An Emerging Approach for Studying Atmospheric Budgets and Chemistry, *Chem. Rev.*, 103, 5025–5048, <https://doi.org/10.1021/cr0206566>, 2003.
- Griffiths, H.: Carbon isotope discrimination and the integration of carbon assimilation pathways in terrestrial CAM plants, *Plant Cell Environ.*, 15, 1051–1062, <https://doi.org/10.1111/j.1365-3040.1992.tb01655.x>, 1992.
- Gromov, S., Jöckel, P., Sander, R., and Brenninkmeijer, C. A. M.: A kinetic chemistry tagging technique and its application to modelling the stable isotopic composition of atmospheric trace gases, *Geosci. Model Dev.*, 3, 337–364, <https://doi.org/10.5194/gmd-3-337-2010>, 2010.
- Gromov, S., Brenninkmeijer, C. A. M., and Jöckel, P.: Fluxes and  $^{13}\text{C}/^{12}\text{C}$  ratios of reactive gas emissions from EMAC EVAL<sub>2</sub> set-up, link to files in NetCDF format, <https://doi.org/10.1594/PANGAEA.877301>, 2017.
- Guenther, A., Hewitt, C. N., Erickson, D., Fall, R., Geron, C., Graedel, T., Harley, P., Klinger, L., Lerdau, M., McKay, W. A., Pierce, T., Scholes, B., Steinbrecher, R., Tallamraju, R., Taylor, J., and Zimmerman, P.: A global model of natural volatile organic compound emissions, *J. Geophys. Res.*, 100, 8873–8892, <https://doi.org/10.1029/94jd02950>, 1995.
- Guo, S., Wen, S., Wang, X., Sheng, G., Fu, J., Hu, P., and Yu, Y.: Carbon isotope analysis for source identification of atmospheric formaldehyde and acetaldehyde in Dinghushan Biosphere Reserve in South China, *Atmos. Environ.*, 43, 3489–3495, <https://doi.org/10.1016/j.atmosenv.2009.04.041>, 2009.
- Ho, K. F., Lee, S. C., Ho, W. K., Blake, D. R., Cheng, Y., Li, Y. S., Ho, S. S. H., Fung, K., Louie, P. K. K., and Park, D.: Vehicular emission of volatile organic compounds (VOCs) from a tunnel study in Hong Kong, *Atmos. Chem. Phys.*, 9, 7491–7504, <https://doi.org/10.5194/acp-9-7491-2009>, 2009.
- IISI: Steel statistical yearbook 2003, International Iron and Steel Institute, Brussels, <http://www.worldsteel.org/en/dam/jcr:c7c68146-a56c-4f33-bac9-68737f6c2242/Steel+statistical+yearbook+2003.pdf> (last access: December 2016), 2004.
- Jöckel, P.: Technical note: Recursive discretisation of geoscientific data in the Modular Earth Submodel System (MESSy), *Atmos. Chem. Phys.*, 6, 3557–3562, <https://doi.org/10.5194/acp-6-3557-2006>, 2006.
- Jöckel, P., Sander, R., Kerkweg, A., Tost, H., and Lelieveld, J.: Technical Note: The Modular Earth Submodel System (MESSy) – a new approach towards Earth System Modeling, *Atmos. Chem. Phys.*, 5, 433–444, <https://doi.org/10.5194/acp-5-433-2005>, 2005.
- Jöckel, P., Tost, H., Pozzer, A., Brühl, C., Buchholz, J., Ganzeveld, L., Hoor, P., Kerkweg, A., Lawrence, M. G., Sander, R., Steil, B., Stiller, G., Tanarhte, M., Taraborrelli, D., van Aardenne, J., and Lelieveld, J.: The atmospheric chemistry general circulation model ECHAM5/MESSy1: consistent simulation of ozone from the surface to the mesosphere, *Atmos. Chem. Phys.*, 6, 5067–5104, <https://doi.org/10.5194/acp-6-5067-2006>, 2006.
- Jöckel, P., Kerkweg, A., Pozzer, A., Sander, R., Tost, H., Riede, H., Baumgaertner, A., Gromov, S., and Kern, B.: Development cycle 2 of the Modular Earth Submodel System (MESSy2), *Geosci. Model Dev.*, 3, 717–752, <https://doi.org/10.5194/gmd-3-717-2010>, 2010.
- Johnke, B.: Emissions from waste incineration, IPCC NGGIP Publication, [http://www.ipcc-nggip.iges.or.jp/public/gp/bgp/5\\_3\\_Waste\\_Incineration.pdf](http://www.ipcc-nggip.iges.or.jp/public/gp/bgp/5_3_Waste_Incineration.pdf) (last access: September 2014), 2000.
- Johnson, B. J. and Dawson, G. A.: A Preliminary Study of the Carbon-Isotopic Content of Ambient Formic Acid and Two Selected Sources: Automobile Exhaust and Formicine Ants, *J. Atmos. Chem.*, 17, 123–140, <https://doi.org/10.1007/BF00702822>, 1993.
- Karl, T., Fall, R., Rosenstiel, T., Prazeller, P., Larsen, B., Seufert, G., and Lindinger, W.: On-line analysis of the  $^{13}\text{CO}_2$  labeling of leaf isoprene suggests multiple subcellular origins of isoprene precursors, *Planta*, 215, 894–905, <https://doi.org/10.1007/s00425-002-0825-2>, 2002.
- Kato, S., Akimoto, H., Bräunlich, M., Röckmann, T., and Brenninkmeijer, C. A. M.: Measurements of stable carbon and oxygen isotopic compositions of CO in automobile exhausts and ambient air from semi-urban Mainz, Germany, *Geochem. J.*, 33, 73–77, <https://doi.org/10.2343/geochemj.33.73>, 1999a.

- Kato, S., Akimoto, H., Röckmann, T., Bräunlich, M., and Brenninkmeijer, C. A. M.: Stable isotopic compositions of carbon monoxide from biomass burning experiments, *Atmos. Environ.*, 33, 4357–4362, [https://doi.org/10.1016/S1352-2310\(99\)00243-5](https://doi.org/10.1016/S1352-2310(99)00243-5), 1999b.
- Kepler, F., Kalin, R. M., Harper, D. B., McRoberts, W. C., and Hamilton, J. T. G.: Carbon isotope anomaly in the major plant  $\text{C}_1$  pool and its global biogeochemical implications, *Biogeosciences*, 1, 123–131, <https://doi.org/10.5194/bg-1-123-2004>, 2004.
- Kepler, F., Harper, D. B., Röckmann, T., Moore, R. M., and Hamilton, J. T. G.: New insight into the atmospheric chloromethane budget gained using stable carbon isotope ratios, *Atmos. Chem. Phys.*, 5, 2403–2411, <https://doi.org/10.5194/acp-5-2403-2005>, 2005.
- Kerkweg, A., Sander, R., Tost, H., and Jöckel, P.: Technical note: Implementation of prescribed (OFFLEM), calculated (ONLEM), and pseudo-emissions (TNUDGE) of chemical species in the Modular Earth Submodel System (MESSy), *Atmos. Chem. Phys.*, 6, 3603–3609, <https://doi.org/10.5194/acp-6-3603-2006>, 2006.
- Kesselmeier, J. and Staudt, M.: Biogenic Volatile Organic Compounds (VOC): An Overview on Emission, Physiology and Ecology, *J. Atmos. Chem.*, 33, 23–88, <https://doi.org/10.1023/a:1006127516791>, 1999.
- Komatsu, D. D., Tsunogai, U., Yamaguchi, J., and Nakagawa, F.: Aselective unsaturated hydrocarbon subtraction technique for stable carbon isotopic analysis of atmospheric methyl chloride, methyl bromide, and  $\text{C}_2$ – $\text{C}_5$  saturated hydrocarbons using continuous-flow isotope ratio mass spectrometry, *Rapid Commun. Mass Sp.*, 19, 477–483, <https://doi.org/10.1002/rcm.1795>, 2005.
- Lassey, K. R., Lowe, D. C., and Manning, M. R.: Thetrend in atmospheric methane  $\delta^{13}\text{C}$  and implications for isotopic constraints on the global methane budget, *Global Biogeochem. Cy.*, 14, 41–49, <https://doi.org/10.1029/1999gb900094>, 2000.
- Lloyd, J. and Farquhar, G. D.:  $^{13}\text{C}$  discrimination during  $\text{CO}_2$  assimilation by the terrestrial biosphere, *Oecologia*, 99, 201–215, <https://doi.org/10.1007/BF00627732>, 1994.
- Manning, M. R., Brenninkmeijer, C. A. M., and Allan, W.: Atmospheric carbon monoxide budget of the southern hemisphere: Implications of  $^{13}\text{C} / ^{12}\text{C}$  measurements, *J. Geophys. Res.*, 102, 10673–10682, <https://doi.org/10.1029/96JD02743>, 1997.
- Nakagawa, F., Tsunogai, U., Gamo, T., and Yoshida, N.: Stable isotopic compositions and fractionations of carbon monoxide at coastal and open ocean stations in the Pacific, *J. Geophys. Res.*, 109, C06016, <https://doi.org/10.1029/2001jc001108>, 2004.
- Nara, H., Nakagawa, F., and Yoshida, N.: Development of two-dimensional gas chromatography/isotope ratio mass spectrometry for the stable carbon isotopic analysis of  $\text{C}_2$ – $\text{C}_5$  non-methane hydrocarbons emitted from biomass burning, *Rapid Commun. Mass Sp.*, 20, 241–247, <https://doi.org/10.1002/rcm.2302>, 2006.
- O'Connor, D.: GHG Emission Reductions From World Biofuel Production And Use, S&T Squared Consultants, Delta, BC, Canada, 16 pp., available at: [http://www.biofuelsassociation.com.au/images/stories/pdf/120809\\_final\\_report\\_ghg.pdf](http://www.biofuelsassociation.com.au/images/stories/pdf/120809_final_report_ghg.pdf) (last access: July 2017), 2009.
- Olivier, J. G. J., Bloos, J. P. J., Berdowski, J. J. M., Visschedijk, A. J. H., and Bouwman, A. F.: A 1990 global emission inventory of anthropogenic sources of carbon monoxide on  $1^\circ \times 1^\circ$  developed in the framework of EDGAR/GEIA, *Chemosphere – Global Change Science*, 1, 1–17, [https://doi.org/10.1016/s1465-9972\(99\)00019-7](https://doi.org/10.1016/s1465-9972(99)00019-7), 1999.
- Olivier, J. G. J., Berdowski, J. J. M., Peters, J. A. H. W., Bakker, J., Visschedijk, A. J. H., and Bloos, J. P. J.: Applications of EDGAR. Including a description of EDGAR 3.2: reference database with trend data for 1970–1995, RIVM, Bilthoven, RIVM report 773301 001/NRP report 410200 051, available at: [www.rivm.nl/bibliotheek/rapporten/410200051.html](http://www.rivm.nl/bibliotheek/rapporten/410200051.html) (last access: March 2015), 2002.
- Popa, M. E., Vollmer, M. K., Jordan, A., Brand, W. A., Pathirana, S. L., Rothe, M., and Röckmann, T.: Vehicle emissions of greenhouse gases and related tracers from a tunnel study:  $\text{CO} : \text{CO}_2$ ,  $\text{N}_2\text{O} : \text{CO}_2$ ,  $\text{CH}_4 : \text{CO}_2$ ,  $\text{O}_2 : \text{CO}_2$  ratios, and the stable isotopes  $^{13}\text{C}$  and  $^{18}\text{O}$  in  $\text{CO}_2$  and  $\text{CO}$ , *Atmos. Chem. Phys.*, 14, 2105–2123, <https://doi.org/10.5194/acp-14-2105-2014>, 2014.
- Pozzer, A., Jöckel, P., Tost, H., Sander, R., Ganzeveld, L., Kerkweg, A., and Lelieveld, J.: Simulating organic species with the global atmospheric chemistry general circulation model ECHAM5/MESSy1: a comparison of model results with observations, *Atmos. Chem. Phys.*, 7, 2527–2550, <https://doi.org/10.5194/acp-7-2527-2007>, 2007.
- Pozzer, A., Jöckel, P., and Van Aardenne, J.: The influence of the vertical distribution of emissions on tropospheric chemistry, *Atmos. Chem. Phys.*, 9, 9417–9432, <https://doi.org/10.5194/acp-9-9417-2009>, 2009.
- Prinn, R. G., Weiss, R. F., Fraser, P. J., Simmonds, P. G., Cunnold, D. M., Alyea, F. N., O'Doherty, S., Salameh, P., Miller, B. R., Huang, J., Wang, R. H. J., Hartley, D. E., Harth, C., Steele, L. P., Sturrock, G., Midgley, P. M., and McCulloch, A.: A history of chemically and radiatively important gases in air deduced from ALE/GAGE/AGAGE, *J. Geophys. Res.*, 105, 17751–17792, <https://doi.org/10.1029/2000jd900141>, 2000.
- Quay, P., Stutsman, J., Wilbur, D., Snover, A., Dlugokencky, E., and Brown, T.: The isotopic composition of atmospheric methane, *Global Biogeochem. Cy.*, 13, 445–461, <https://doi.org/10.1029/1998gb900006>, 1999.
- Randerson, J. T., van der Werf, G. R., Collatz, G. J., Giglio, L., Still, C. J., Kasibhatla, P., Miller, J. B., White, J. W. C., DeFries, R. S., and Kasischke, E. S.: Fire emissions from  $\text{C}_3$  and  $\text{C}_4$  vegetation and their influence on interannual variability of atmospheric  $\text{CO}_2$  and  $\delta^{13}\text{CO}_2$ , *Global Biogeochem. Cy.*, 19, GB2019, <https://doi.org/10.1029/2004gb002366>, 2005.
- Randerson, J. T., van der Werf, G. R., Giglio, L., Collatz, G. J., and Kasibhatla, P. S.: Global Fire Emissions Database, Version 2 (GFED v2.1), Oak Ridge National Laboratory Distributed Active Archive Center, Oak Ridge, Tennessee, USA, available at: <http://daac.ornl.gov/> (last access: September 2014), 2007.
- Röckmann, T., Jöckel, P., Gros, V., Bräunlich, M., Possnert, G., and Brenninkmeijer, C. A. M.: Using  $^{14}\text{C}$ ,  $^{13}\text{C}$ ,  $^{18}\text{O}$  and  $^{17}\text{O}$  isotopic variations to provide insights into the high northern latitude surface  $\text{CO}$  inventory, *Atmos. Chem. Phys.*, 2, 147–159, <https://doi.org/10.5194/acp-2-147-2002>, 2002.
- Rudolph, J.: Biogenic sources of atmospheric alkenes and acetylene, in: Biogenic Volatile Organic Compounds in the Atmosphere – Summary of Present Knowledge, edited by: Helas, G., Slanina, S., and Steinbrecher, R., SPB Academic Publishers, Amsterdam, The Netherlands, 53–65, 1997.

- Rudolph, J., Czuba, E., Norman, A. L., Huang, L., and Ernst, D.: Stable carbon isotope composition of nonmethane hydrocarbons in emissions from transportation related sources and atmospheric observations in an urban atmosphere, *Atmos. Environ.*, 36, 1173–1181, [https://doi.org/10.1016/S1352-2310\(01\)00537-4](https://doi.org/10.1016/S1352-2310(01)00537-4), 2002.
- Rudolph, J., Anderson, R. S., Czapiewski, K. V., Czuba, E., Ernst, D., Gillespie, T., Huang, L., Rigby, C., and Thompson, A. E.: The Stable Carbon Isotope Ratio of Biogenic Emissions of Isoprene and the Potential Use of Stable Isotope Ratio Measurements to Study Photochemical Processing of Isoprene in the Atmosphere, *J. Atmos. Chem.*, 44, 39–55, <https://doi.org/10.1023/a:1022116304550>, 2003.
- Sander, R., Baumgaertner, A., Gromov, S., Harder, H., Jöckel, P., Kerkweg, A., Kubistin, D., Regelin, E., Riede, H., Sandu, A., Taraborrelli, D., Tost, H., and Xie, Z.-Q.: The atmospheric chemistry box model CAABA/MECCA-3.0, *Geosci. Model Dev.*, 4, 373–380, <https://doi.org/10.5194/gmd-4-373-2011>, 2011.
- Sanderson, M. G.: Emission of Carbon Monoxide by Vegetation and Soils, available <https://library.metoffice.gov.uk/M10326UK/OPAC/Details/Record.aspx?BibCode=14947676> (last access: December 2016), 2002.
- Saueressig, G., Crowley, J. N., Bergamaschi, P., Brühl, C., Brenninkmeijer, C. A. M., and Fischer, H.: Carbon 13 and D kinetic isotope effects in the reactions of  $\text{CH}_4$  with  $\text{O}(^1\text{D})$  and  $\text{OH}$ : New laboratory measurements and their implications for the isotopic composition of stratospheric methane, *J. Geophys. Res.*, 106, 23127–23138, <https://doi.org/10.1029/2000jd000120>, 2001.
- Saurer, M., Prévôt, A. S. H., Dommen, J., Sandradewi, J., Baltensperger, U., and Siegwolf, R. T. W.: The influence of traffic and wood combustion on the stable isotopic composition of carbon monoxide, *Atmos. Chem. Phys.*, 9, 3147–3161, <https://doi.org/10.5194/acp-9-3147-2009>, 2009.
- Schmitt, A. and Brunner, B.: Emissions from aviation and their development over time, in: Final Report on the BMBF Verbundprogramm, Schadstoffe in der Luftfahrt, edited by: Schumann, U., Chlond, A., Ebel, A., Kärcher, B., Pak, H., Schlager, H., Schmitt, A., and Wendling, P., Deutsches Zentrum für Luft- und Raumfahrt, Oberpfaffenhofen and Cologne, Germany, DLR-Mitteilung 97-04, 37–52, 1997.
- Schnitzler, J.-P., Graus, M., Kreuzwieser, J., Heizmann, U., Rennenberg, H., Wisthaler, A., and Hansel, A.: Contribution of Different Carbon Sources to Isoprene Biosynthesis in Poplar Leaves, *Plant Physiol.*, 135, 152–160, <https://doi.org/10.1104/pp.103.037374>, 2004.
- Scholze, M., Kaplan, J. O., Knorr, W., and Heimann, M.: Climate and interannual variability of the atmosphere-biosphere  $^{13}\text{C}$  flux, *Geophys. Res. Lett.*, 30, 1097, <https://doi.org/10.1029/2002gl015631>, 2003.
- Scholze, M., Ciais, P., and Heimann, M.: Modeling terrestrial  $^{13}\text{C}$  cycling: Climate, land use and fire, *Global Biogeochem. Cy.*, 22, GB1009, <https://doi.org/10.1029/2006gb002899>, 2008.
- Sharkey, T. D., Loreto, F., Delwiche, C. F., and Treichel, I. W.: Fractionation of Carbon Isotopes during Biogenesis of Atmospheric Isoprene, *Plant Physiol.*, 97, 463–466, <https://doi.org/10.1104/pp.97.1.463>, 1991.
- Soja, A. J., Cofer, W. R., Shugart, H. H., Sukhinin, A. I., Stackhouse Jr., P. W., McRae, D. J., and Conard, S. G.: Estimating fire emissions and disparities in boreal Siberia (1998–2002), *J. Geophys. Res.*, 109, D14S06, <https://doi.org/10.1029/2004jd004570>, 2004.
- Stein, O. and Rudolph, J.: Modeling and interpretation of stable carbon isotope ratios of ethane in global chemical transport models, *J. Geophys. Res.*, 112, D14308, <https://doi.org/10.1029/2006jd008062>, 2007.
- Stein, O., Schultz, M. G., Bouarar, I., Clark, H., Huijnen, V., Gaudel, A., George, M., and Clerbaux, C.: On the wintertime low bias of Northern Hemisphere carbon monoxide found in global model simulations, *Atmos. Chem. Phys.*, 14, 9295–9316, <https://doi.org/10.5194/acp-14-9295-2014>, 2014.
- Stevens, C. M. and Wagner, A. F.: The Role of Isotope Fractionation Effects in Atmospheric Chemistry, *Z. Naturforsch. A*, 44a, 376–384, 1989.
- Stevens, C. M., Walling, D., Venters, A., Ross, L. E., Engelkemeir, A., and Krout, L.: Isotopic Composition of Atmospheric Carbon Monoxide, *Earth Planet. Sc. Lett.*, 16, 147–165, [https://doi.org/10.1016/0012-821X\(72\)90183-5](https://doi.org/10.1016/0012-821X(72)90183-5), 1972.
- Still, C. J., Berry, J. A., Collatz, G. J., and DeFries, R. S.: Global distribution of  $\text{C}_3$  and  $\text{C}_4$  vegetation: Carbon cycle implications, *Global Biogeochem. Cy.*, 17, 1006, <https://doi.org/10.1029/2001gb001807>, 2003.
- Tarantola, A.: Inverse Problem Theory and Methods for Model Parameter Estimation, Other Titles in Applied Mathematics, Society for Industrial and Applied Mathematics, 342 pp., 2005.
- Thompson, A., Anderson, R., Rudolph, J., and Huang, L.: Stable carbon isotope signatures of background tropospheric chloromethane and  $\text{CFC}_{113}$ , *Biogeochemistry*, 60, 191–211, <https://doi.org/10.1023/a:1019820208377>, 2002.
- Tipple, B. J. and Pagani, M.: The Early Origins of Terrestrial  $\text{C}_4$  Photosynthesis, *Annu. Rev. Earth Pl. Sc.*, 35, 435–461, <https://doi.org/10.1146/annurev.earth.35.031306.140150>, 2007.
- Vallet, C., Masud, Z., and Martin, M. L.: Isotopic characterization of the bioconversion of lactose into ethanol, *Food Chem.*, 63, 115–123, [https://doi.org/10.1016/S0308-8146\(97\)00218-5](https://doi.org/10.1016/S0308-8146(97)00218-5), 1998.
- van Aardenne, J. A., Dentener, F., Olivier, J. G. G., Peters, J. A. H. W., and Ganzeveld, L. N.: The EDGAR3.2 Fast Track 2000 dataset (32FT2000), Joint Research Centre, Institute for Environment and Sustainability (JRC-IES), Climate Change Unit, TP280, 21020, Ispra (Va), Italy, available at: <http://www.mnp.nl/edgar/model/v32ft2000edgar/docv32ft2000/> (last access: March 2015), 2005.
- van der Werf, G. R., Randerson, J. T., Giglio, L., Collatz, G. J., Kasibhatla, P. S., and Arellano Jr., A. F.: Interannual variability in global biomass burning emissions from 1997 to 2004, *Atmos. Chem. Phys.*, 6, 3423–3441, <https://doi.org/10.5194/acp-6-3423-2006>, 2006.
- Yakir, D.: The paper trail of the  $^{13}\text{C}$  of atmospheric  $\text{CO}_2$  since the industrial revolution period, *Environ. Res. Lett.*, 6, 034007, <https://doi.org/10.1088/1748-9326/6/3/034007>, 2011.
- Yamada, K., Hattori, R., Ito, Y., Shibata, H., and Yoshida, N.: Carbon isotopic signatures of methanol and acetaldehyde emitted from biomass burning source, *Geophys. Res. Lett.*, 36, L18807, <https://doi.org/10.1029/2009GL038962>, 2009.
- Yamada, K., Hattori, R., Ito, Y., Shibata, H., and Yoshida, N.: Determination of carbon isotope ratios of methanol and acetaldehyde in air samples by gas chromatography-isotope ratio mass spectrometry combined with headspace solid-

- phase microextraction, *Isot. Environ. Health S.*, 46, 392–399, <https://doi.org/10.1080/10256016.2010.505686>, 2010.
- Yevich, R. and Logan, J. A.: An assessment of biofuel use and burning of agricultural waste in the developing world, *Global Biogeochem. Cy.*, 17, 1095, <https://doi.org/10.1029/2002gb001952>, 2003.
- Yokelson, R. J., Susott, R., Ward, D. E., Reardon, J., and Griffith, D. W. T.: Emissions from smoldering combustion of biomass measured by open-path Fourier transform infrared spectroscopy, *J. Geophys. Res.*, 102, 18865–18877, <https://doi.org/10.1029/97jd00852>, 1997.
- Zhang, B.-L., Fallourd, V., Role, C., and Martin, G. J.: Comparison of isotopic fractionation in lactic acid and ethanol fermentations, *Bioorg. Chem.*, 31, 227–236, [https://doi.org/10.1016/S0045-2068\(03\)00051-8](https://doi.org/10.1016/S0045-2068(03)00051-8), 2003.
- Zhang, Q. L., Chang, T. L., and Li, W. J.: A Calibrated Measurement of the Atomic Weight of Carbon, *Chinese Science Bulletin*, 35, 290–296, 1990.